Effect of Pressure Rate on Rate and State Frictional Slip

John W. Rudnicki[1,1,1] and Yatai Zhan[2,2,2]

[1]Northwestern University
[2]University of Science and Technology Beijing

November 30, 2022

Abstract

This paper analyzes the effects of pore pressure rate for a spring - block system that is a simple model of a laboratory experiment. Pore pressure is increased at a constant rate in a remote reservoir and slip is governed by rate and state friction. The frequency of rapid slip events increases with the increase of a nondimensional pressure rate that is the ratio of the time scale of frictional sliding to that for pressure increase. As the pressure rate increases, the more rapid increase of pore pressure on the slip surface quickly stabilizes slip events due to rate and state friction. Rate and state and pressure rate effects interact in a limited range of pressure rate and diffusivity. This range includes pressure rates and diffusivities representative of recent laboratory experiments.

Effect of Pressure Rate on Rate and State Frictional Slip

J. W. Rudnicki[1],Y. Zhan[2]

[1]Department of Civil and Environmental Engineering and Department of Mechanical Engineering, Northwestern University, Evanston, IL 60208-3109
[2]School of Civil and Resource Engineering, University of Science and Technology Beijing, No. 30, Xueyuan Road, Haidian District, Beijing, 100083, P. R. China

Key Points:

- At low pressure rates instabilities are due to rate and state friction
- At high pressure rates failure occurs based on the Coulomb law with the effective stress principle
- Pressure rate affects the type,frequency, and magnitude of slip events

Corresponding author: J. W. Rudnicki, `jwrudn@northwestern.edu`

Abstract

This paper analyzes the effects of pore pressure rate for a spring - block system that is a simple model of a laboratory experiment. Pore pressure is increased at a constant rate in a remote reservoir and slip is governed by rate and state friction. The frequency of rapid slip events increases with the increase of a nondimensional pressure rate that is the ratio of the time scale of frictional sliding to that for pressure increase. Rate and state and pressure rate effects interact in a limited range of pressure rate and diffusivity. Above a critical value of the pressure rate there is transition to a significant downward linear trend of the stress, reflecting the increase of pore fluid pressure in the reservoir. This trend leads to Coulomb failure due to the decrease of the frictional resistance and the effective stress principle.

Plain Language Summary

Recent field observations have identified fluid injection as an important factor in causing the dramatic increase of earthquakes in the central US and recent laboratory experiments have observed effects of fluid pressure rate on frictional sliding. This paper studies a simple model of a laboratory experiment: a block resting on a frictional surface and pulled by a spring. The frictional resistance to sliding depends on the rate and history of sliding. Fluid pressure is increased at a constant rate at a distance remote from the surface. The paper calculates the types and characteristics of rapid slip events and their dependence on the pressure rate and how fast fluid can diffuse from the reservoir to the frictional surface.

1 Introduction

Increases in pore fluid pressure are an important mechanism to promote failure (slip) on fault surfaces. According to the Coulomb condition the frictional resistance is given by

$$\tau = \mu_0 (\sigma - p) \tag{1}$$

where μ_0 is a friction coefficient, σ is the normal stress on the frictional surface and p is the pore fluid pressure. The pore fluid pressure reduces the effective normal stress (normal stress minus pore fluid pressure) and thereby reduces the frictional resistance. Slip, which could be seismic or aseismic, is predicted to occur when the applied shear stress equals the resistance.

This mechanism has been suggested as playing an important role in a variety of geologic processes. Much recent attention on the effects of pore fluid on failure has been stimulated by the dramatic increase of earthquakes in the mid-continental US (Ellsworth, 2013). Most of these events appear to be associated with the injection of waste water from hydraulic fracturing (Horton, 2012; Keranen et al., 2013, 2014; Weingarten et al., 2015; Barbour et al., 2017; Goebel et al., 2017) There is not yet any clear understanding of why these earthquakes do or do not occur and whether induced slip wil be seismic or aseismic. The nearness of stress on faults to a critical value, the orientation and location of faults relative to injection sites, and availability of permeability channels are certainly factors. Operational factors that affect the incidence of seismicity include the volume of fluids injected or withdrawn and the injection rate (Ellsworth, 2013).

Weingarten et al. (2015) examined about 20,000 wells in the mid-continent US associated with seismicity and found that among various operational parameters, the injection rate had the best correlation with induced seismicity. A computational study by Almakari et al. (2019) examined the effect of pore pressure rate on seismicity. They simulated the seismicity rate increase due to a ramp increase in pore pressure on a heterogeneous fault. They found that a sharp increase in the seismicity rate correlates with the pore pressure rate for a wide range of injection pressure and that the maximum seismicity rate increases with the pore pressure rate.

Although field observations are the ultimate test of the effects of pore fluid on failure, their interpretation is often complicated by uncertainty about the boundary conditions, state of stress, heterogeneity of hydrologic and mechanical structure, and history. Laboratory experiments, despite their limited size and time scales, offer a more controlled environment that can contribute insight into fundamental processes.

Recent laboratory studies addressing the role of pressure rate in causing slip are those of French et al. (2016), Passelégue et al. (2018), Cappa et al. (2019) and Noël et al. (2019). The primary motivation for this study is the experiments by French et al. (2016). They did axisymmetric compression tests with saw cuts on two sandstones, Berea and Darley Dale. In addition to standard axisymmetric compression tests, they did tests in which the confining stress was reduced or the pore pressure in the reservoir connected to the sample was increased at a constant rate. In some tests, they did both. They found that instability (accelerated slip events) did not occur unless they decreased the confining stress (lateral relaxation tests). When they did get instability, the total slip, slip velocity and shear stress drops of events were better correlated with the pore pressure rate (in the reservoir) than with the magnitude of the pore pressure itself.

This paper extends the spring - block model of Segall and Rice (1995) (Figure 1) to examine the effect of pressure rate. The spring - block system is an oversimplied model of crustal faulting, but it is a reasonable idealization of laboratory experiments in which slip occurs nearly simultaneously on the frictional surface. Segall and Rice (1995) showed that this system exhibits a wide spectrum of behavior that is further enriched by including the pressure rate. Despite the limitations of the model for crustal faulting, among their results are a constraint on the maximum pore pressure at depth that is consistent with the absence of an observed heat flow anomaly and the occurrence of aftershock-like instabilities.

The goal of this study is to examine the role of imposed pore pressure rate on frictional slip. The calculations are not meant to be a faithful simulation of the experiment of French et al. (2016) but their observations are used as a guide. Although French et al. (2016) discuss some of their results in terms of rate and state (hereafter abbreviated RS) friction, they do not infer any RS parameters from their experiments. Nevertheless, we use RS friction because of its strong observational basis and wide use in fault models. The results can aid in the interpretation of laboratory tests and, to a lesser extent, field studies.

2 Formulation

The model is that of Segall and Rice (1995) shown in Figure 1. A block of unit area subjected to a constant normal stress σ slides on a thin porous layer. The block is connected to a spring with stiffness k. Slip of the block is u. The other end of the spring is displaced at a constant rate v_0. Thus, the shear stress due to motion of the block is

$$\tau = k\,(v_0 t - u) \tag{2}$$

The layer has porosity ϕ and a pore pressure p. There is a flux of fluid to the layer from a remote reservoir with a pore pressure p_∞. The remote reservoir is at some nominal distance L from the layer. Consistent with the discrete spring-mass system, Segall and Rice (1995) adopt the approximation of Rudnicki and Chen (1988) that the fluid mass flux into the layer is proportional to the difference between the remote pore pressure p_∞ and the pore pressure in the layer. Consequently the equation expressing conservation of fluid mass is

$$c^*\,(p_\infty - p) = \dot{p} + \dot{\phi}/\beta \tag{3}$$

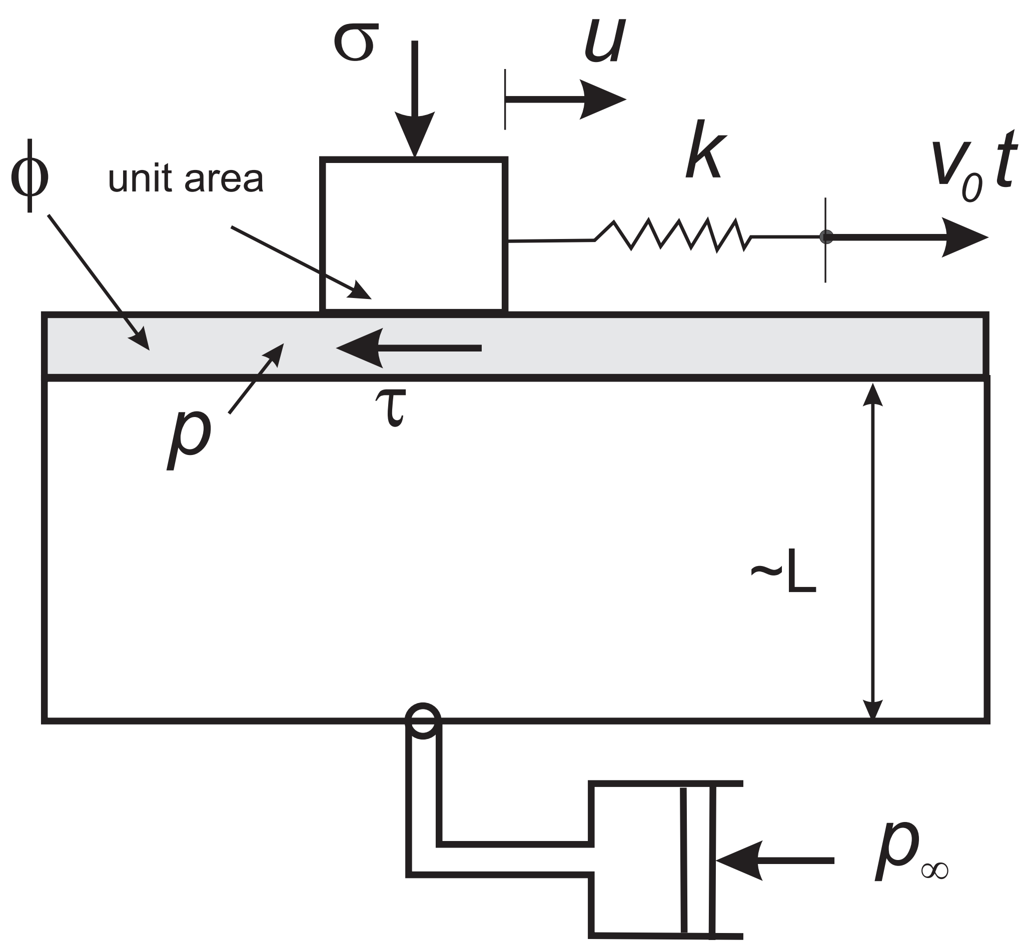

Figure 1. The spring - block model of Segall and Rice (1995)

where ϕ is now the inelastic part of the porosity, the superposed dot denotes the time derivative and c^* is the reciprocal of a time constant for fluid diffusion. c^* can be expressed in terms of a diffusivity c as $c^* = c/L^2$. $\beta = \phi_0(\beta_f + \beta_\phi)$ is a compressibility where β_f is the compressibility of the pore fluid, β_ϕ is the compressibility of the pore space and ϕ_0 is the initial porosity. In an extension of Segall and Rice (1995) we take the far-field pore pressure to increase linearly with time:

$$p_\infty = p_\infty^0 + \dot{p}_\infty t \tag{4}$$

Slip on the layer is described by RS friction (Dieterich, 1979; Ruina, 1983) of the form

$$\tau = (\sigma - p)\left[\mu_0 + a\ln(v/v_0) + b\,(\theta/\theta_0)\right] \tag{5}$$

where μ_0 is the nominal friction coefficient, $v = du/dt$ is the slider velocity, and θ is a state variable. Reference values of the velocity and state are v_0 and θ_0 and a and b are constitutive parameters. Two versions of the equation for the evolution of state are typically used: the “slip” law and the “aging” or “slowness” law. Segall and Rice (1995) use the “aging”law:

$$\dot{\theta} = 1 - \theta v/d_c \tag{6}$$

where d_c is a characteristic sliding distance.

If the block has been steadily sliding at a velocity V_1 and the velocity is suddenly changed to a velocity $V_2 > V_1$, the friction suddenly increases by $a\ln(V_2/V_1)$ and then decays over a characteristic distance d_c to a new steady state level $(b-a)\ln(V_2/V_1)$. For $b - a > 0$ the new steady state level is less than the old and the response is velocity weakening. For $b-a < 0$ the response is velocity strengthening. Ruina (1983) showed that for velocity weakening the response can be unstable, in the sense that small perturbations grow exponentially in time, when the spring stiffness is less than a critical value given by

$$k_{crit} = (\sigma - p)(b - a)/d_c \tag{7}$$

Note that the pore pressure can affect stability in two ways. In (7) an increase in pore pressure reduces k_{crit}. However an increase in pore pressure reduces the frictional resistance according to (5). Because the magnitudes of a and b are small compared with μ_0, the difference between the magnitudes of (5) and (1) is small. Hence, when the pore pressure increases sufficiently to reduce the frictional resistance below the applied shear stress, failure essentially occurs according to (1). We refer to this as a Coulomb failure. The simulations will show that there is a transition from RS instability according to (7) to Coulomb failure with increasing pressure rate.

Segall and Rice (1995) proposed the following evolution equation for the porosity:

$$\dot{\phi} = -(\phi - \phi_{ss})\,v/d_c \tag{8}$$

where the steady state value is given by $\phi_{ss} = \phi_0 + \varepsilon\ln(v/v_0)$. The initial value of the porosity is ϕ_0 and ε is a parameter that gives the magnitude of the effect. They show that this formulation describes well the data of Marone et al. (1990) on porosity changes with shear of simulated fault gouge and find that $\epsilon = 1.7 \times 10^{-4}$.

The final ingredient is the equation of motion:

$$\dot{\tau} = k\,(v_0 - v) - \eta\dot{v} \tag{9}$$

The second term on the right employs the radiation damping approximation to inertia, i.e. mdv/dt is replaced by ηv where $\eta = G/2v_s$. G is the shear modulus and v_s is the shear wave velocity (Rice & Tse, 1986; Rice, 1993).

Differentiating (5) and setting equal to (9) along with (3), (6), and (8) yield a system of four ordinary differential equations for V, p, θ, and ϕ. It is advantageous to rewrite these equations in the non-dimensional variables $V = v/v_0$, $T = v_0 t/d_c$, $\Sigma = \mu_0\,(1 - p/\sigma)$, $P = p/\sigma$, $\hat{\eta} = \eta v_0/\sigma$, $\hat{c} = c^* d_c/v_0$, $\hat{\beta} = \sigma\beta$, $\hat{\theta} = \theta v_0/d_c$, $\hat{\phi} = \phi - \phi_0$ and $\hat{k} = k/k_c$ where k_c is the critical stiffness (7) based on the initial value of the far-field pore pressure p^0_∞. With these non-dimensionalizations $\dot{P}_\infty = \dot{p}_\infty d_c/v_0\sigma$.

3 Parameter Values

Although the model is simple, there are a quite a few parameters. Some of these are uncertain and others vary widely. In the simulations, we will vary two non-dimensional parameters, $\dot{P}_\infty$ and $\hat{c}$ to focus on the roles of the pressure rate and diffusivity. To the extent possible, we choose values representative of the experiments of French et al. (2016). In Table 1, they give imposed slip rates ranging from 1.6×10^{-7} to 4.6×10^{-7} m/s for Berea and 1.6×10^{-7} to 6.5×10^{-7} m/s for Darley Dale. We take $v_0 = 3.0 \times 10^{-7}$ m/sas representative. Lateral confining stresses range from 42 to 62 MPa and we take $\sigma = 50$ MPa. The initial value of the pore pressure is about 10 MPa. This gives $P^0_\infty = 0.2$. Using $v_s = 2.5 \times 10^3$ m/s (Green & Wang, 1994) and $G = 10^4$ MPa gives $\hat{\eta} \approx 10^{-8}$. Pore pressure rates vary from 0.3 to 1.0 MPa/min.

French et al. (2016) give 10^{-14} m^2 and 10^{-13}m^2 for the permeabilities of Berea and Darley Dale, respectively. The diffusivity is given by $c = k\gamma/\nu S$ where k is the permeability, γ is the weight density of water (9.81×10^4 Pa), ν is the kinematic viscosity of water (10^{-3} Pa s) and S is a storage coefficient, equal to 1.5×10^{-6} m^{-1} (Green & Wang, 1994). These values give $c = 0.065$ m^2/s for Berea. Dividing by the square of the specimen length (50.8 mm) gives $c^* = 25.2$ s^{-1}.

Although French et al. (2016) discuss their results in terms of RS friction, they do not measure the parameters in their experiment. Segall and Rice (1995) infer $d_c = 0.02$mm and $\epsilon = 1.7\times10^{-4}$ from the experiments of Marone et al. (1990) and $\beta = 1.4\times10^{-4}$MPa^{-1} from experiments of Zoback and Byerlee (1976) and we use these. Using the larger of the pressure rates (1 MPa/min), $v_0 = 3.0 \times 10^{-7}$m/s, and $d_c = 0.02$ mm gives $\dot{P}_\infty = 0.022$.

In addition, we adopt the representative RS frictional parameters used by Segall and Rice (1995), $a = 0.010$ and $b = 0.015$, and take the nominal coefficient as $\mu_0 = 0.64$ (French et al., 2016). Because $a < b$, the behavior is velocity weakening and a critical value of the stiffness is given by (7). In their experiments, French et al. (2016) induce instability (resulting in rapid slip events) by reducing the lateral confining stress leading to a reduction of normal stress on the slip surface. For simplicity and in order to focus on the role of the pressure rate, we keep the normal stress σ constant and examine the response for values of the stiffness less than the critical value for drained deformation given by (7). In particular, we arbitrarily take $\hat{k} = 0.1$. (Results for $\hat{k} = 0.5$ are shown in the Supporting Information).

Segall and Rice (1995) derive an expression critical stiffness as a function of the non-dimensional diffusivity $\hat{c}$. When expressed as the ratio to the critical stiffness for drained deformation, (7), the result is

$$K(\hat{c}) = 1 - \frac{\epsilon\mu_0}{\beta(\sigma - p)(b - a)} F(\hat{c}) \tag{10}$$

where $F(\hat{c}) \to 0$ as $\hat{c} \to \infty$, corresponding to very rapid diffusion and drained conditions (pore pressure equal to that in the reservoir), and $F(\hat{c}) \to 1$ as $\hat{c} \to 0$, corresponding to very slow diffusion and undrained conditions (no change in fluid mass).

For the values of parameters of the experiment, $c = 0.065$ m^2/s, $v_0 = 3.0\times10^{-7}$ m/s and $d_c = 0.02$ mm, $\hat{c} = 1.68\times10^3$ and from (10) $K \approx 1$, indicating that deforma-

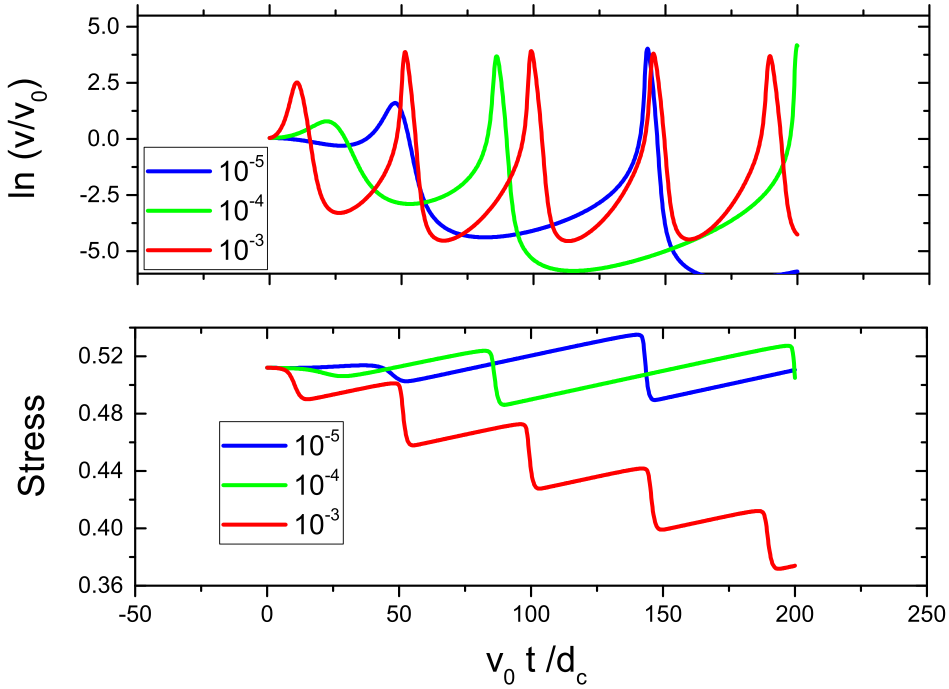

Figure 2. Upper panel shows logarithm of velocity (divided by v_0) and lower panel shows stress (divided by σ), $\Sigma = \mu_0 (1 - p/\sigma)$, for three values of $\hat{P}_\infty$: 10^{-5}, 10^{-4} and 10^{-3} The abscissa is $T = v_0 t/d_c$ and $\hat{c} = 1$.

tion is essentially drained. However, French et al. (2016) cite Zhang and Tullis (1998) in arguing that permeabilities could be as small as 10^{-17} m^2 for gouge layers formed by frictional shearing of surfaces and Wibberley and Shimamoto (2003) have found permeabilities as low as 10^{-19}m^2 in samples from the fault core of the Median Tectonic Line. These give values of $\hat{c}$ three to five orders of magnitude smaller.

4 Simulations

The simulations are started with a small perturbation from steady sliding: $v(0) = 1.05v_0$. Other initial conditions are as follows: $\tau(0) = \mu_0 \left(\sigma - p^0_\infty\right)$, $p = p^0_\infty$, $\hat{\phi} = 0$, and $\hat{\theta} = v_0/v(0)$. Results are shown for $\hat{k} = 0.1$, three values of $\dot{P}_\infty$, 10^{-5}, 10^{-4}, and 10^{-3}, and two values of $\hat{c}$: 1.0 (Figure 2) and 10 (Figure 3). The upper panel of Figure 2 shows a series of rapid slip events. If the first event is ignored (because it appears to be affected by the initial conditions), the maximum slip velocity is about 40 ($e^{3.7}$) times the imposed velocity. For $\dot{P}_\infty = 10^{-3}$, there are three events with periods about 45 but only the first, at $T \approx 52$, is within the duration of the experiment $T = 60$ (corresponding to about 4000 s). For $\dot{P}_\infty = 10^{-5}$ and 10^{-4} only one event (again ignoring the first) occurs within the duration of the simulation. The bottom panel shows the stress. Drops occur simultaneously with the slip events. For $\dot{P}_\infty = 10^{-3}$ the stress drop is about 0.04 (a dimensional stress drop of $0.04 \times \sigma = 2$ MPa). For $\dot{P}_\infty = 10^{-4}$ the stress drop is slightly smaller and slight larger for $\dot{P}_\infty = 10^{-5}$. For values of $\dot{P}_\infty$ less than 10^{-5} the effect of the pore pressure rate is minimal and the response is nearly entirely due to RS effects. For 10^{-3} the downward trend reflects the linear increase in pore fluid pressure

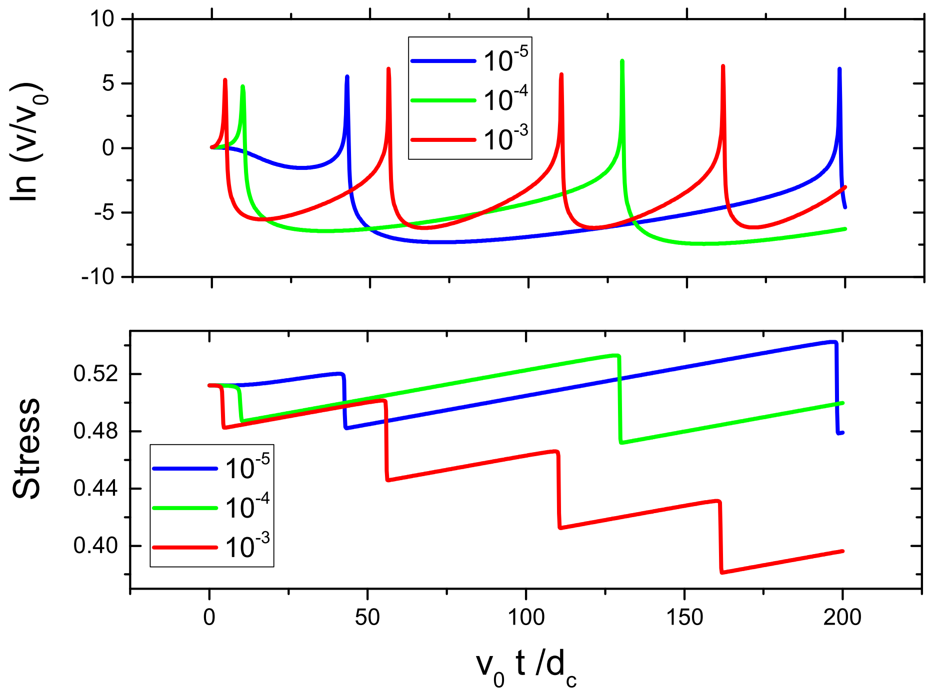

Figure 3. Same as Figure 2 for $\hat{c} = 10$.

in the reservoir. This increase reduces the nominal frictional resistance, $\mu_0 (\sigma - p)$, and tends toward a Coulomb failure.

Figure 3 shows results for $\hat{c} = 10$. For $\dot{P}_\infty = 10^{-3}$ the peak velocities ($e^5 = 155$) and the stress drops are larger (0.05) and the time between events is longer (52) than for $\hat{c} = 1$ For $\dot{P}_\infty = 10^{-4}$ and 10^{-5}, the magnitude of the peak velocity and stress drop are slightly larger. If, again, the first slip event is ignored, during the duration of the experiment only one event occurs for $\dot{P}_\infty = 10^{-3}$ and none for 10^{-4} and 10^{-5}. As in Figure 2, there is a transition at $\dot{P}_\infty = 10^{-3}$ to a significant downward trend of the stress that eventually will reduce the frictional resistance to zero. According to (10), for $\hat{c} = 10$, the ratio of the critical stiffness to the critical stiffnes for drained deformation (both based on the pore pressure p_∞^0) $K = 0.938$. Therefore, $\hat{c} = 10$ is close to drained conditions and there will be little difference in the response for larger values of $\hat{c}$. For $\hat{c} = 1$, $K = 0.51$, which is much closer to undrained response and, according to Figure 4 of Segall and Rice (1995), is in a range where $K(\hat{c})$ decreases rapidly with $\ln(\hat{c})$. For the parameters here undrained deformation is stable and the response is increasingly damped for smaller values of $\hat{c}$. Thus, the smaller peak velocities and stress drops in Figure 2, $\hat{c} = 1$, compared with Figure 3, $\hat{c} = 10$, reflect the stabilizing effects of dilatant hardening for conditions closer to undrained deformation. (Results for $\hat{c} = 0.1$ are shown in Supporting Information.)

For $\dot{P}_\infty = 10^{-2}$, representative of the laboratory value, the frictional resistance decreases to zero before the end of the simulation ($T = 200$) but does not for $T = 60$, corresponding to the duration of the experiment. Figure 4 shows the response for two values of $\hat{c}$: 1 and 10. For the larger diffusivity there are 11 slip events with slightly decreasing maximum slip rates. For $\hat{c} = 1$, there is a single slow event followed by strongly damped oscillations. For smaller diffusivities, the response is even more strongly damped.

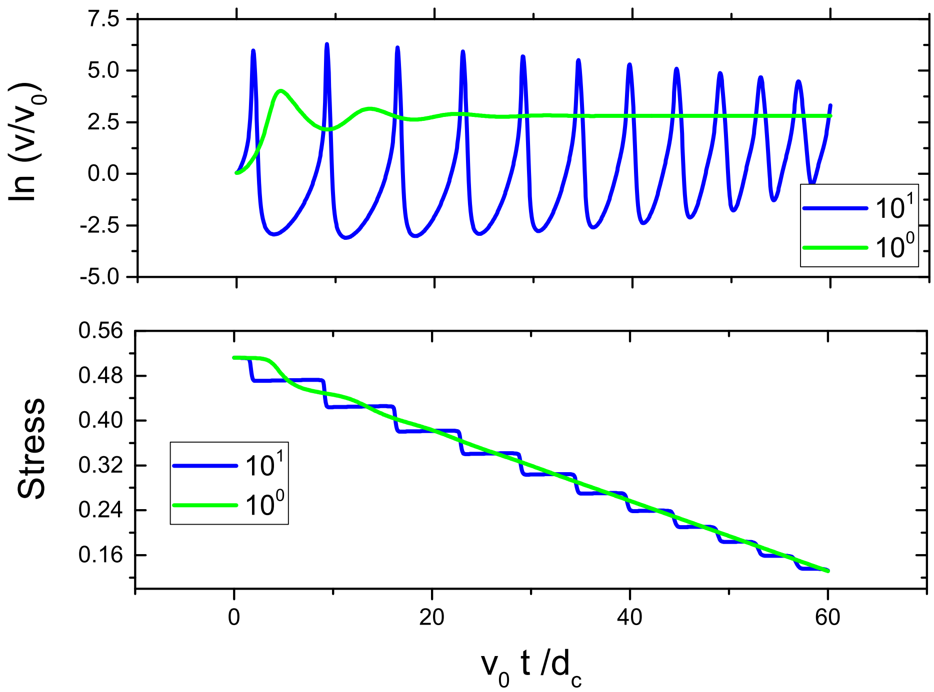

Figure 4. Same as Figure 2 for $\dot{P}_\infty = 10^{-2}$ and $\hat{c} = 1$ and 10.

The lower panel shows that the relatively rapid increase of pressure causes a steep, linear downward trend of the stress that will reach zero shortly after $T = 60$.

5 Discussion

The simulations illustrate the effects of $\dot{P}_\infty$, the ratio of the characteristic time of the imposed rate of frictional slip to that of pressurization. For all the values of $\hat{c}$ and $\hat{k}$ considered, the frequency of events increases with $\dot{P}_\infty$. Also, in all cases, between $\dot{P}_\infty = 10^{-4}$ and 10^{-3} there is transition to a significant downward linear trend of the stress, reflecting the linear increase of pore fluid pressure in the reservoir. This trend leads to Coulomb failure due to the decrease of the frictional resistance according to the effective stress principle. For $\dot{P}_\infty$ within the range of 10^{-5} to 10^{-3} the interaction of RS effects and the increase of pore pressure is most significant. For values smaller than about 10^{-5} the pressure rate has relatively little effect and the occurrence of slip events is dominated by RS effects.

The response also depends on $\hat{c}$, the ratio of the characteristic time of the imposed rate of frictional slip to that of fluid diffusion. The magnitude of the stress drop and peak velocities decrease with decreasing $\hat{c}$. The decrease is most dramatic for $\hat{c} = 0.1$, reflecting the stabilizing effect of dilatant hardening as undrained conditions are approached. This stabilizing effect begins to dominate for $\hat{c}$ less than about 1. For $\hat{c}$ greater than about 10 conditions are effectively drained and largely independent of $\hat{c}$. Despite the simplicity of the model, these results inform the range of parameters for which different effects dominate and indicate a transition from RS instability to Coulomb failure with increasing $\dot{P}_\infty$.

Although the spring-slider system is a reasonable approximation of a laboratory test, the calculations here cannot be considered a faithful simulation of the experiments of French et al. (2016). A major difference is that for simplicity and to isolate the effect of the reservoir pressure rate we have taken the normal stress as constant. In their experiments French et al. (2016) alter the normal stress and, in addition, the normal stress changes with slip on the frictional surface. Rudnicki and Chen (1988) have used a slip-weakening model to examine the interaction of pore pressure effects with normal stress changes in experiments by Brace and Martin (1968) and Chambon and Rudnicki (2001) extended Segall and Rice (1995) to include normal stress changes. Neither of these studies included the pore pressure rate changes or the rate and state effect of changes in the normal stress identified by Linker and Dieterich (1992). Although it has been suggested that the latter effects are small (Segall & Rice, 1995; Chambon & Rudnicki, 2001), He and Wong (2014) have shown that they can significantly affect the slip velocities for state evolution described by the slip law.

French et al. (2016) give some interpretation of their results in terms of RS effects but they do not measure values of the parameters a, b and d_c and the appropriate values are uncertain. Marone et al. (1990) conducted velocity stepping experiments on gouge layers of Ottawa sand and the value of $d_c = 0.02$ mm, inferred by Segall and Rice (1995) from their experiments, is probably reasonable for a sandstone. For a and b we have simply used representative magnitudes with $b > a$ in order to have velocity weakening and instability. It is quite possible and, perhaps, even likely that $b < a$ and instability is induced by changes in normal stress. Furthermore, there are indications that the values of a, b and d_c change with pore pressure and imposed slip rate (Scuderi & Collettini, 2016; Noël et al., 2019; Cappa et al., 2019).

In spite of the differences between the model and the experiment of French et al. (2016) the calculated stress drops, maximum slip rates and number of events are consistent with those observed in the experiments. For $\hat{c} = 10$ and $\dot{P}_\infty = 10^{-3}$ maximum slip rates are about two orders of magnitude greater than v_0, in rough agreement with the experiment (Figure 3d of French et al. (2016)). Similarly, stress drops from the calculations are similar to those in the experiments. Stress drops from Figure 4c of French et al. (2016) are 0.5 to 2.0 MPa. In the calculations they are slightly larger, about 2.0 to 4.0 MPa (0.04 to 0.05 $\times$50 MPa). In addition, the single slip event predicted during the experiment is consistent with the observations. Admittedly, this agreement is based on the arbitrary choice of $\hat{k} = 0.1$. The response for $\hat{k} = 0.5$ is not anything like the experiment (See Supporting Information.)

There are, however, some clear discrepancies between the experiment and the simulations. French et al. (2016) observe a pore pressure increase, indicating compaction, accompanies slip instability. The magnitude of the decrease is about 55 % of the shear stress drop and the increase is permanent. The simulations show a decrease of pressure with instability and then an increase with magnitude much smaller than observed in the experiment. One possible explanation is that the (nondimensional) pressure rate in the experiment is about 10^{-2} at which we find that Coulomb failure begins to dominate RS effects. Compaction and dilation in the formulation here, and in Segall and Rice (1995), are entirely associated with RS effects. The compaction observed by French et al. (2016) could be associated with slip due to the decreasing Coulomb resistance. Alternatively, it may be due to the neglect of normal stress changes in the simulations.

Another experiment imposing a pore pressure rate is that of Noël et al. (2019). They impose a sinusoidal pressure variation with period $t_0 = 102$ s and amplitudes 1 to 8 MPa on a faulted Fontainebleu sandstone. The confining pressure is 30 or 45 MPa, the axial displacement rate is 10^{-3} or 10^{-4} mm/s and d_c decreases from $4{\times}10^{-3}$ to 10^{-3} mm over a velocity range 10^{-5} to 10^{-2} mm/s. Calculating the maximum pressure rate for an amplitude of 1 MPa, a confining stress of 40 MPa, $v_0 = 10^{-4}$ mm/s and $d_c = 10^{-3}$ mm gives $\dot{P}_\infty$ in the range 0.015 to 0.120. At the higher displacement rate $\dot{P}_\infty$ is an order of magnitude higher. They find $c^* > 1$ s^{-1} and using the same values of d_c and v_0 gives $\hat{c} > 10$, corresponding to effectively drained conditions. The range of $\dot{P}_\infty$ is where the Coulomb failure dominates instability due to rate and state effects. These estimates are consistent with their conclusion that slip instabilities correspond to Coulomb failure and that larger amplitudes induce the instability earlier.

The spring mass system is a primitive model of faulting. Realistic models of in situ slip would include the propagation of slip, inhomogenity of stress and flux of pore fluid along the failure surface (e.g, Garagash and Germanovich (2012), Bhattacharya and Viesca (2019), Cappa et al. (2019)). Nevertheless, we can make some connection with the study of Almakari et al. (2019). They simulate slip on a heterogeneous fault governed by rate and state friction and examine the seismicity rate increase due to a ramp increase in pore pressure at an injection site. The rates range from 0.01 to 10 MPa/d. They find that the seismicity rate increases with both pore pressure and rate, but that the effect of the rate is greater. Almakari et al. (2019) use $\sigma = 100$ MPa and $v_0 = 10^{-9}$ m/s. Their values of d_c vary along the fault and range from 0.01 to 0.37 mm. Using a value of $d_c = 0.1$ mm, in the middle of this range, a pressure rate 10 MPa/d and the values of σ and v_∞ yield $\dot{P}_\infty = 0.012$. This is about the same as for the French et al. (2016) experiment and at the upper range of where there is a competition between slip events due to rate and state friction and a Coulomb failure.

6 Conclusion

We have investigated the system of a spring and a mass sliding on a surface governed by rate and state friction. The pore pressure on the surface is coupled to the value in a remote reservoir. As Segall and Rice (1995) have shown, the model, although very simple, has a rich range of responses. The effects of increasing pore pressure in the reservoir further enrich this range. The analysis is motivated by observations that induced seismicity depends on injection rate and, more specifically, by experiments of French et al. (2016). The simulations illustrate the effects of pressure rate and diffusivity on the type, magnitude, frequency, and stress drop of instabilites. In addition, they identify a particular pressure rate at which RS instabilites transition to Coulomb failure. This pressure rate is similar to those imposed in some experiments and at least one field simulation. Although the spring block configuration is simple, these simulations can aid in the interpretation of experiments and provide guidance for field studies.

Acknowledgments

No new data was used in this manuscript. Y.Z. thanks the University of Science and Technology Beijing for support and Northwestern University for hosting him during his visit from July 1, 2018 to January 1, 2019.

References

Almakari, M., Dublanchet, P., Hervé, C., & Frédéric, P. (2019). Effect of the injection scenario on the rate and magnitudecontent of injection-induced seismicity:case of a heterogeneous fault. *Journal of Geophysical Research*, *124*, 8426-8448. doi: https://doi.org/10.1029/2019jb017898

Barbour, A. J., Norbeck, J. H., & Rubinstein, J. L. (2017). The effects of varying injection rates in Osage County, Oklahoma, on the 2016 Mw 5.8 Pawnee earthquake. *Seismological Research Letters*, *140-153*(4), 38.

Bhattacharya, P., & Viesca, R. C. (2019). Fluid-induced aseismic fault slip outpaces pore-fluid migration. *Science*, *364*, 464-468. doi: 10.1126/science.aaw7354

Brace, W. F., & Martin, R. J., III. (1968). A test of the law of effective stress for crystalline rocks of low porosity. *International Journal of Rock Mechanics and*

Mining Sciences, *5*, 415-426.

Cappa, F., Scuderi, M. M., Collettini, C., Guglielmi, Y., & Avouac, J.-P. (2019). Stabilization of fault slip by fluid injection in the laboratory and in situ. *Science Advances*, *5*(eaau4065). doi: 10.1126/sciadv.aau4065

Chambon, G., & Rudnicki, J. W. (2001). Effects of normal stress variations on frictional stability of a fluid-infiltrated fault. *Journal of Geophysical Research*, *106*(B6), 11,353-11,372.

Dieterich, J. H. (1979). Modeling of rock friction, 1, experimental results and constitutive equations. *Journal of Geophysical Research*, *84*, 2161-2168.

Ellsworth, W. L. (2013). Injection-induced earthquakes. *Science*, *341*. doi: 10.1126/science.1225942

French, M. E., Zhu, W., & Banker, J. (2016). Fault slip controlled by stress path and fluid pressurization rate. *Geophysical Research Letters*, *43*, 4330-4339. doi: doi:10.1002/2016GL068893

Garagash, D. I., & Germanovich, L. N. (2012). Nucleation and arrest of dynamic slip on a pressurized fault. *Journal of Geophysical Research*, *117*(B10319). doi: 10.1029/2012JB009209

Goebel, T. H. W., Weingarten, M., X., C., Haffener, J., & Brodsky, E. E. (2017). The 2016 Mw 5.1 Fairview, Oklahoma earthquakes: Evidence for long-range poroelastic triggering at > 40 km from fluid disposal wells. *Earth and Planetary Science Letters*, *472*, 50-61. doi: http://dx.doi.org/10.1016/j.epsl.2017.05.011

Green, D. H., & Wang, H. F. (1994). Shear wave velocity and attenuation from pulse-echo studies of Berea sandstone. *Journal of Geophysical Research*, *99*(B6), 11755 - 11763. doi: 10:10.1029/94JB00506

He, C., & Wong, T.-F. (2014). Effect of varying normal stress on stability and dynamic motion of a spring - slider system with rate- and state- dependent friction. *Earthquake Science*, *27*, 577-587. doi: 10.1007/s11589-014-0098-4

Horton, S. (2012). Disposal of hydrofracking waste fluid by injection into subsurface aquifers triggers earthquake swarm in central Arkansas with potential for damaging earthquake. *Seismological Research Letters*, *83*(2), 250-260. doi: doi:10.1785/gssrl.83.2.250

Keranen, K. M., Savage, H. M., Abers, G. A., & Cochran, E. S. (2013). Potentially induced earthquakes in Oklahoma, USA: Links between wastewater injection and the 2011 Mw 5.7 earthquake sequence. *Geology*, *41*(6), 699-702. doi: doi:10.1130G34045.1

Keranen, K. M., Weingarten, M., Abers, G. A., Bekins, B. A., & Ge, S. (2014). Sharp increase in central Oklahoma seismicity since 2008 induced by massive wastewater injection. *Science*, *345*(6195), 448-451. doi: doi:10.1126/science.1255802

Linker, M. F., & Dieterich, J. H. (1992). Effects of variable normal stress on rock friction: observations and constitutive equations. *Journal of Geophysical Research*, *97*, 4923-4940.

Marone, C., Raleigh, C. B., & Scholz, C. H. (1990). Frictional behavior and constitutive modeling modeling of simulated fault gouge. *Journal of Geophysical Research*, *95*, 7007 - 7025.

Noël, C., Passelégue, F. X., Giorgetti, C., & Violay, M. (2019). Fault reactivation during fluid pressure oscillations: Transition from stable to unstable slip. *Journal of Geophysical Research*, *124*, 10,940-10,953. doi: https://doi.org/10.1029/2019JB018517

Passelégue, F. X., Brantut, N., & Mitchell, T. M. (2018). Fault reactivation by fluid injection: controls from stress state and injection rate. *Geophysical Research Letters*, *45*, 12,837-12846. doi: https://doi.org/10.1029/2018GL080470

Rice, J. R. (1993). Spatio-temporal complexity of slip on a fault. *Journal of Geophysical Research*, *98*(B6), 9885-9907.

Rice, J. R., & Tse, S. T. (1986). Dynamic motion of a single degree of freedom system following a rate and state dependent friction law. *Journal of Geophysical Research*, *91*(B1), 521-530.

Rudnicki, J. W., & Chen, C.-H. (1988). Stabilization of rapid frictional slip on a weakening fault by dilatant hardening. *Journal of Geophysical Research*, *93*, 4745-4757.

Ruina, A. (1983). Slip instability and state variable friction laws. *Journal of Geophysical Research*, *88*, 10,359-10,370.

Scuderi, M. M., & Collettini, C. (2016). The role of fluid pressure in induced vs. triggered seismicity: insights from rock deformation experiments on carbonates. *Nature Scientific Reports*. doi: 10.1038/srep24852

Segall, P., & Rice, J. R. (1995). Dilatancy, compaction, and slip instability of a fluid-infliltrated fault. *Journal of Geophysical Research*, *100*(B11), 22155-22171.

Weingarten, M., Ge, S., Godt, J. W., Bekins, B. A., & Rubinstein, J. L. (2015). High-rate injection is associated with the increase in U.S. mid-continent seismicity. *Science*, *348*(6241), 1336-1340.

Wibberley, C. A. J., & Shimamoto, T. (2003). Internal structure and permeability of major fault zones: The Median Tectonic Line in Mie Prefecture, Southwest Japan. *Journal of Structural Geology*, *25*, 49-78.

Zhang, S., & Tullis, T. (1998). The effect of fault slip on permeability and permeability anisotropy in quartz gouge. *Tectonophysics*, *298*(1-2), 41-52.

Zoback, M. D., & Byerlee, J. D. (1976). Effect of high-pressure on permeability of Ottawa sand. *American Association of Petroleum Geologists Bulletin*, *60*, 1531-1542.

Effect of Pressure Rate on Rate and State Frictional Slip

J. W. Rudnicki[1],Y. Zhan[2]

[1]Department of Civil and Environmental Engineering and Department of Mechanical Engineering, Northwestern University, Evanston, IL 60208-3109
[2]School of Civil and Resource Engineering, University of Science and Technology Beijing, No. 30, Xueyuan Road, Haidian District, Beijing, 100083, P. R. China

Key Points:

- Slip instabilities occur during the duration of a representative experiment in a limited range of pressure rate and diffusivity
- Identifies a pressure rate above which slip events are strongly damped by a rapid decrease of effective stress
- Interaction between fluid diffusion and pressure rate affects the type, frequency, and magnitude of slip events

Corresponding author: J. W. Rudnicki, `jwrudn@northwestern.edu`

Abstract

This paper analyzes the effects of pore pressure rate for a spring - block system that is a simple model of a laboratory experiment. Pore pressure is increased at a constant rate in a remote reservoir and slip is governed by rate and state friction. The frequency of rapid slip events increases with the increase of a nondimensional pressure rate that is the ratio of the time scale of frictional sliding to that for pressure increase. As the pressure rate increases, the more rapid increase of pore pressure on the slip surface quickly stabilizes slip events due to rate and state friction. Rate and state and pressure rate effects interact in a limited range of pressure rate and diffusivity. This range includes pressure rates and diffusivities representative of recent laboratory experiments.

Plain Language Summary

Recent field observations have identified fluid injection as an important factor in causing the dramatic increase of earthquakes in the central US and recent laboratory experiments have observed effects of fluid pressure rate on frictional sliding. This paper studies a simple model of a laboratory experiment: a block resting on a frictional surface and pulled by a spring. The frictional resistance to sliding depends on the rate and history of sliding. Fluid pressure is increased at a constant rate at a distance remote from the surface. The paper calculates the types and characteristics of rapid slip events and their dependence on the pressure rate and how fast fluid can diffuse from the reservoir to the frictional surface.

1 Introduction

Recent attention on the effects of pore fluid on failure has been stimulated by the dramatic increase of earthquakes in the mid-continental US (Ellsworth, 2013). Most of these events appear to be associated with the injection of waste water from hydraulic fracturing (Horton, 2012; Keranen et al., 2013, 2014; Weingarten et al., 2015; Barbour et al., 2017; Goebel et al., 2017) There is not yet any clear understanding of why these earthquakes occur and whether induced slip will be seismic or aseismic. The nearness of stress on faults to a critical value, the orientation and location of faults relative to injection sites, and availability of permeability channels are certainly factors. Operational factors that affect the incidence of seismicity include the volume of fluids injected or withdrawn and the injection rate (Ellsworth, 2013).

Two indications of the importance of the pressure rate come from a field study and a numerical simulation. Weingarten et al. (2015) examined about 20,000 wells in the mid-continent US associated with seismicity and found that among various operational parameters, the injection rate had the best correlation with induced seismicity. Almakari et al. (2019) examined the effect of pore pressure rate on seismicity. They simulated the seismicity rate increase due to a ramp increase in pore pressure on a heterogeneous fault. They find that the seismicity rate increases with both pore pressure and rate, but that the effect of the rate is greater.

Although field observations are the ultimate test of the effects of pore fluid on failure, their interpretation is often complicated by uncertainty about the boundary conditions, state of stress, heterogeneity of hydrologic and mechanical structure, and history. Laboratory experiments, despite their limited size and time scales, offer a more controlled environment that can contribute insight into fundamental processes.

The motivation for this study is recent laboratory studies addressing the role of pressure rate in causing slip (French et al., 2016; Scuderi et al., 2017; Passelégue et al., 2018; Cappa et al., 2019; Noël et al., 2019; Wang et al., 2020). Three of these studies (French

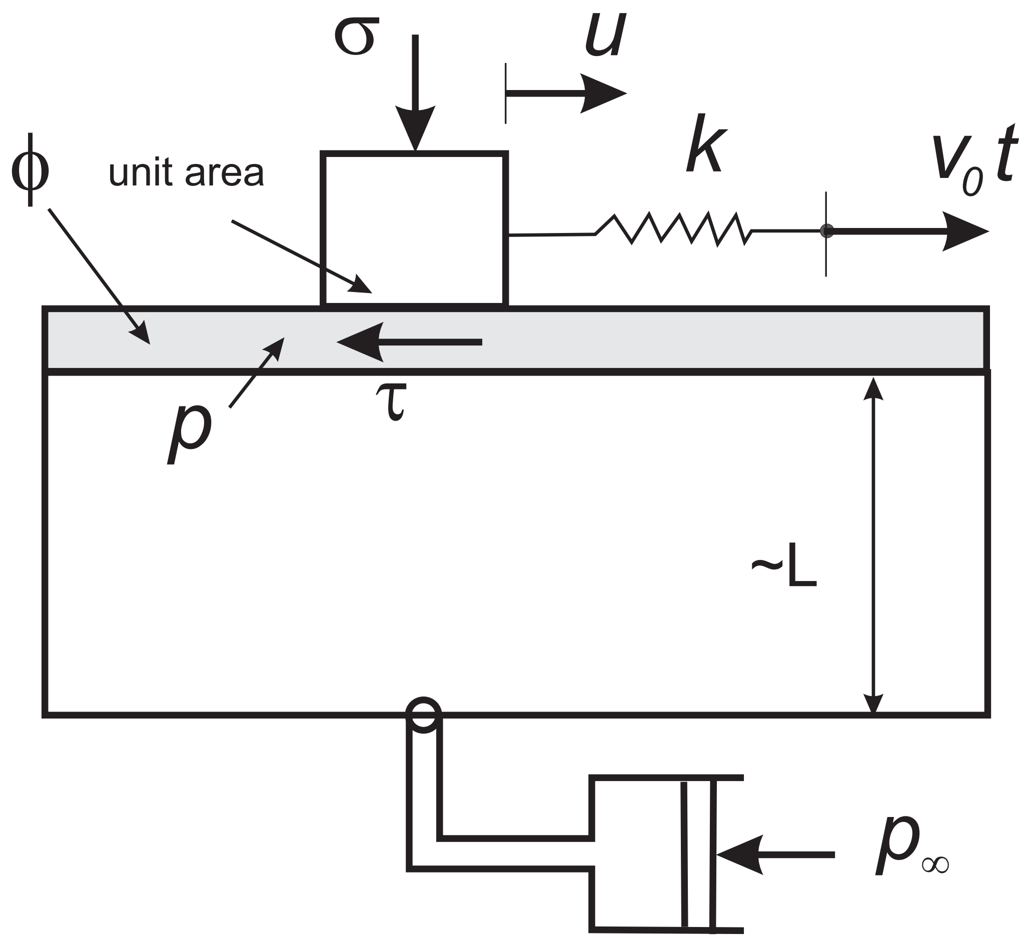

Figure 1. The spring - block model of Segall and Rice (1995)

et al., 2016; Passelégue et al., 2018; Wang et al., 2020) indicate that the pressure rate is more important than the pore pressure itself in failure.

This paper extends the spring - block model of Segall and Rice (1995) (Figure 1) to examine the effect of pressure rate. This system is an oversimplified model of crustal faulting, but it is a reasonable idealization of laboratory experiments in which slip occurs nearly simultaneously on the frictional surface. Segall and Rice (1995) showed that this system exhibits a wide spectrum of behavior that is further enriched by including the pressure rate. Despite the limitations of the model for crustal faulting, among their results are a constraint on the maximum pore pressure at depth that is consistent with the absence of an observed heat flow anomaly and the occurrence of aftershock-like instabilities.

In Segall and Rice (1995) sliding of the block on a porous layer is governed by rate and state (hereafter abbreviated RS) friction. In the last 50 years, an enormous amount of experimental work (Marone, 1998) has documented that a RS formulation is an accurate description of rock friction. In this formulation, friction depends on the sliding velocity and a variable that characterizes the state of the surface. Simulations using RS friction describe many observed features of earthquakes.

The goal of this study is to examine the effect of imposed pore pressure rate on RS frictional slip in a simple situation that avoids complicating effects. In particular, we examine the case of constant pore pressure rate with imposed displacement. We focus on the effects of the interaction of the time scales of fluid diffusion, pore pressure rate, and RS frictional slip on type, magnitude and frequency of slip events. The results can aid in the interpretation of laboratory tests and, to a lesser extent, field studies.

2 Formulation

The model is that of Segall and Rice (1995) shown in Figure 1. A block of unit area subjected to a constant normal stress σ slides on a thin porous layer. The block is connected to a spring with stiffness k. Slip of the block is u. The other end of the spring is displaced at a constant rate v_0. Thus, the shear stress due to motion of the block is

$$\tau = k\left(v_0 t - u\right) \tag{1}$$

The layer has porosity ϕ and a pore pressure p. There is a flux of fluid to the layer from a remote reservoir with a pore pressure p_∞. The remote reservoir is at some nominal distance L from the layer. Consistent with the discrete spring-mass system, Segall and Rice (1995) adopt the approximation of Rudnicki and Chen (1988) that the fluid mass flux into the layer is proportional to the difference between the remote pore pressure p_∞ and the pore pressure in the layer. Consequently the equation expressing conservation of fluid mass is

$$c^*\left(p_\infty - p\right) = \dot{p} + \dot{\phi}/\beta \tag{2}$$

where ϕ is now the inelastic part of the porosity, the superposed dot denotes the time derivative and c^* is the reciprocal of a time constant for fluid diffusion. c^* can be expressed in terms of a diffusivity c as $c^* = c/L^2$. $\beta = \phi_0\left(\beta_f + \beta_\phi\right)$ is a compressibility where β_f is the compressibility of the pore fluid, β_ϕ is the compressibility of the pore space and ϕ_0 is the initial porosity. In an extension of Segall and Rice (1995) we take the far-field pore pressure to increase linearly with time:

$$p_\infty = p_\infty^0 + \dot{p}_\infty t \tag{3}$$

Slip on the layer is described by RS friction (Dieterich, 1979; Ruina, 1983) of the form

$$\tau = (\sigma - p)\left[\mu_0 + a\ln\left(v/v_0\right) + b\left(\theta/\theta_0\right)\right] \tag{4}$$

where μ_0 is the nominal friction coefficient, $v = du/dt$ is the slider velocity, and θ is a state variable. Reference values of the velocity and state are v_0 and θ_0 and a and b are constitutive parameters. Two versions of the equation for the evolution of state are typically used: the "slip" law and the "aging" or "slowness" law. Bhattacharya et al. (2015) have shown that the slip law fits experimental data better, particularly at larger velocity steps. Consequently, we use the slip law:

$$\dot{\theta} = -\left(v\theta/d_c\right)\ln\left(v\theta/d_c\right) \tag{5}$$

where d_c is a characteristic sliding distance.

For $b - a > 0$ the response is velocity weakening. For $b - a < 0$ the response is velocity strengthening. Ruina (1983) showed that for velocity weakening the response can be unstable, in the sense that small perturbations grow exponentially in time, when the spring stiffness is less than a critical value k_{crit}. For drained response (constant pore pressure corresponding to rapid fluid diffusion),

$$k_{crit} = \left(\sigma - p\right)\left(b - a\right)/d_c \tag{6}$$

Note that an increase in pore pressure reduces k_{crit} and, thus, stabilizes response.

Segall and Rice (1995) proposed the following evolution equation for the porosity:

$$\dot{\phi} = -\left(\phi - \phi_{ss}\right) v/d_c \quad (7)$$

where the steady state value is given by $\phi_{ss} = \phi_0 + \varepsilon \ln\left(v/v_0\right)$. The initial value of the porosity is ϕ_0 and ε is a parameter that gives the magnitude of the effect. They show that this formulation describes well the data of Marone et al. (1990) on porosity changes with shear of simulated fault gouge and find that $\epsilon = 1.7 \times 10^{-4}$.

The final ingredient is the equation of motion:

$$\dot{\tau} = k\left(v_0 - v\right) - \eta \dot{v} \quad (8)$$

The second term on the right employs the radiation damping approximation to inertia, i.e. mdv/dt is replaced by ηv where $\eta = G/2v_s$. G is the shear modulus and v_s is the shear wave velocity (Rice & Tse, 1986; Rice, 1993).

Differentiating (4) and setting equal to (8) along with (2), (5), and (7) yield a system of four ordinary differential equations for V, p, θ, and ϕ. It is advantageous to rewrite these equations in the non-dimensional variables $V = v/v_0$, $T = v_0 t/d_c$, $\Sigma = \mu_0\left(1 - p/\sigma\right)$, $P = p/\sigma$, $\hat{\eta} = \eta v_0/\sigma$, $\hat{c} = c^* d_c/v_0$, $\hat{\beta} = \sigma\beta$, $\hat{\theta} = \theta v_0/d_c$, $\hat{\phi} = \phi - \phi_0$ and $\hat{k} = k/k_c$ where k_c is the critical stiffness (6) based on the initial value of the far-field pore pressure p^0_∞. With these non-dimensionalizations $\dot{P}_\infty = \dot{p}_\infty d_c/v_0\sigma$.

3 Parameter Values

Although the model is simple, there are a quite a few parameters. Some of these are uncertain and others vary widely. In the simulations, we will vary two non-dimensional parameters, $\dot{P}_\infty$ and $\hat{c}$. We choose values representative of the experiments of French et al. (2016) for Berea and Darley Dale sandstones. These are similar to those for the Fontainebleau sandstone used by Noël et al. (2019). In Table 1, French et al. (2016) give imposed slip rates ranging from 1.6×10^{-7} to 6.5×10^{-7} m/s. We take $v_0 = 3.0\times10^{-7}$ m/s as representative. Lateral confining stresses range from 42 to 62 MPa and we take $\sigma = 50$ MPa. The initial value of the pore pressure is about 10 MPa. This gives $P^0_\infty = 0.2$. Using $v_s = 2.5 \times 10^3$ m/s (Green & Wang, 1994) and $G = 10^4$ MPa gives $\hat{\eta} \approx 10^{-8}$. Pore pressure rates vary from 0.3 to 1.0 MPa/min.

French et al. (2016) give 10^{-14} m^2 and 10^{-13} m^2 for the permeabilities of the two sandstones. The diffusivity is given by $c = k\gamma/\nu S$ where k is the permeability, γ is the weight density of water (9.81×10^4 Pa), ν is the dynamic viscosity of water (10^{-3} Pa s) and S is a storage coefficient, equal to 1.5×10^{-6} m^{-1} (Green & Wang, 1994). These values give $c = 0.065$ m^2/s for Berea. Dividing by the square of the specimen length (50.8 mm) gives $c^* = 25.2$ s^{-1}.

Although French et al. (2016) discuss their results in terms of RS friction, they do not measure the parameters in their experiment. From their experiments on simulated fault gouge, Marone et al. (1990) find $d_c = 0.02$ mm. For this value of d_c and v_0, the duration of the experiment (approximately 4000 s) corresponds to $T = 60$. For values used by Segall and Rice (1995) as representative of crustal faulting, $d_c = 0.01$ m and $v_0 = 0.03$ m/year, $T = 100$ corresponds to 33.3 years.

Segall and Rice (1995) infer $\epsilon = 1.7 \times 10^{-4}$ from the experiments of Marone et al. (1990) and $\beta = 1.4\times10^{-4}$MPa^{-1} from experiments of Zoback and Byerlee (1976). We use these. Using the larger of the pressure rates (1 MPa/min), $v_0 = 3.0\times10^{-7}$m/s, and $d_c = 0.02$ mm gives $\dot{P}_\infty = 0.022$.

In addition, we adopt the representative RS frictional parameters used by Segall and Rice (1995), $a = 0.010$ and $b = 0.015$, and take the nominal friction coefficient as $\mu_0 = 0.64$ (French et al., 2016). Because $a < b$, the behavior is velocity weakening and a critical value of the stiffness for drained deformation is given by (6) . In their experiments, French et al. (2016) induce instability (resulting in rapid slip events) by reducing the lateral confining stress leading to a reduction of normal stress on the slip surface. For simplicity and in order to focus on the role of the pressure rate, we keep the normal stress σ constant and choose a value for the stiffness much less than the critical value for drained deformation (6). In particular, we arbitrarily take $\hat{k} = 0.1$. (Results for $\hat{k} = 0.5$ are shown in the Supporting Information).

Segall and Rice (1995) derive an expression for the critical stiffness as a function of the non-dimensional diffusivity $\hat{c}$. The ratio of the critical stiffness to that for drained deformation (6) is

$$K(\hat{c}) = 1 - \frac{\epsilon\mu_0}{\beta(\sigma - p)(b - a)} F(\hat{c}) \tag{9}$$

where $F(\hat{c}) \to 0$ as $\hat{c} \to \infty$, corresponding to very rapid diffusion and drained conditions (pore pressure equal to that in the reservoir), and $F(\hat{c}) \to 1$ as $\hat{c} \to 0$, corresponding to very slow diffusion and undrained conditions (no change in fluid mass).

For the values of parameters of the experiment, $c = 0.065$ m^2/s, $v_0 = 3.0 \times 10^{-7}$ m/s and $d_c = 0.02$ mm, $\hat{c} = 1.68 \times 10^3$ and from (9) $K \approx 1$, indicating that deformation is essentially drained. However, French et al. (2016) cite Zhang and Tullis (1998) in arguing that permeabilities could be as small as 10^{-17} m^2 for gouge layers formed by frictional shearing of surfaces and Wibberley and Shimamoto (2003) have found permeabilities as low as 10^{-19} m^2 in samples from the fault core of the Median Tectonic Line. These give values of $\hat{c}$ three to five orders of magnitude smaller.

4 Simulations

The simulations are started with a small perturbation from steady sliding: $v(0) = 1.05\ v_0$. Other initial conditions are as follows: $\tau(0) = \mu_0\left(\sigma - p^0_\infty\right)$, $p = p^0_\infty$, $\hat{\phi} = 0$, and $\hat{\theta} = v_0/v(0)$. Results are shown for $\hat{k} = 0.1$, two values of $\dot{P}_\infty$, 10^{-3} and 10^{-4}, and two values of the diffusivity, $\hat{c}$: 1.0 (Figure 2) and 10 (Figure 3). Figure 4 shows results for $\dot{P}_\infty = 10^{-2}$ and two values of the diffusivity, $\hat{c} = 1.0$ and $\hat{c} = 10$.

If the first peak in Figure 2 is ignored (because it appears to be affected by the initial conditions), the maximum slip velocity for both pressure rates is about 30 ($e^{3.4}$) v_0 times the imposed velocity. For $\dot{P}_\infty = 10^{-3}$, the first event occurs at about $T \approx 50$ which is slightly before the end of the experiment of French et al. (2016), $T = 60$. Thereafter, the velocity peaks decay to $\approx 2.5\ v_0$ (slightly greater than v_0 because of the pressure rate). The initial period is $T \approx 37$ which decreases with time. The decay occurs because the increasing pressure reduces the effective stress (bottom panel) and, consequently, the value of k_{crit} (6), to zero at $T \approx 800$. For $\dot{P}_\infty = 10^{-4}$, the first event (again ignoring the initial peak) occurs at about 80. Thereafter, peaks of roughly similar magnitude occur with a period of about 93. The is no discernible decay in the magnitude of the peaks in slip but, because of the increasing pressure, the slip rate eventually decays to near v_0 but not until about at about $T \approx 8000$. The bottom panel shows the (non-dimensional) effective stress multiplied by μ_0. Because the total normal stress is constant, changes in stress reflect pore pressure changes of the opposite sign. Drops occur simultaneously with the slip events. For $\dot{P}_\infty = 10^{-3}$ the maximum stress drop is about 0.04 (a dimensional stress drop of $0.04 \times \sigma/\mu_0 = 3.1$ MPa). For $\dot{P}_\infty = 10^{-4}$ the stress drop is about the same. For values of $\dot{P}_\infty$ less than 10^{-4} the effect of the pore pressure change in the reservoir is minimal and the response is nearly entirely due to RS effects.

Figure 3 shows results for $\hat{c} = 10$. For $\dot{P}_\infty = 10^{-3}$ the maximum peak velocities ($e^{5.7} = 300$) is much greater than for $\hat{c} = 1$, the maximum stress drop is about the same (0.04) and the time between events is smaller (44). Again ignoring the first peak,

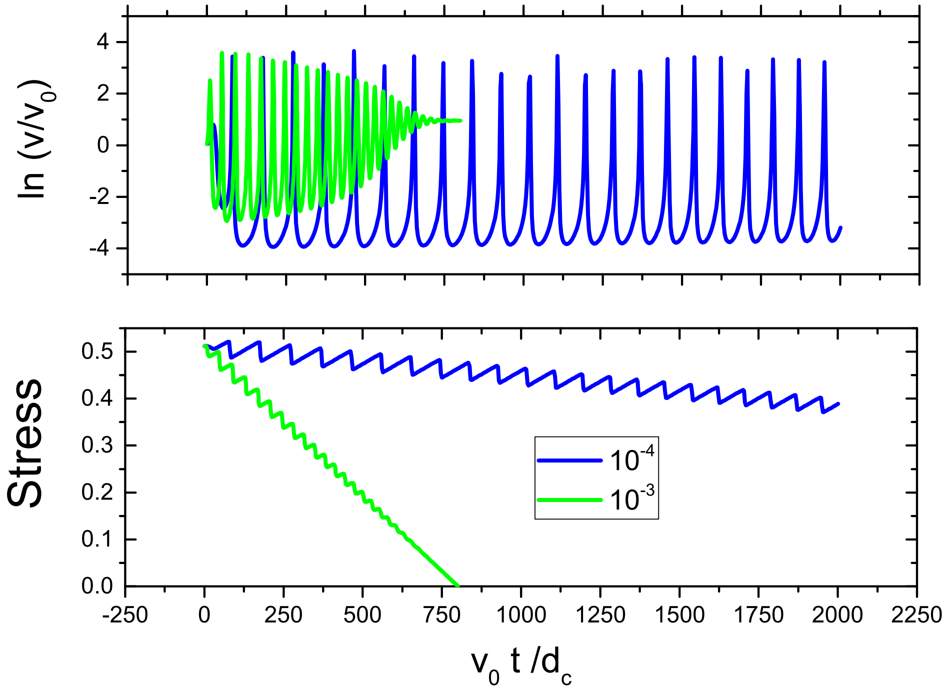

Figure 2. Upper panel shows logarithm of velocity (divided by v_0) and lower panel shows stress (divided by σ), $\Sigma = \mu_0 (1 - p/\sigma)$, for two values of $\hat{P}_\infty$: 10^{-4}, and 10^{-3} The abscissa is $T = v_0 t/d_c$ and $\hat{c} = 1$.

the first event occurs at $T \approx 50$. For $\dot{P}_\infty = 10^{-4}$, the magnitude of the peak velocities vary but with no obvious pattern. They do, however, eventually decay to near v_0 but, again, not until about $T \approx 8000$. The stress drops are slightly larger (0.46). If, again, the first slip event is ignored, the first peak occurs at $T = 108$.

According to (9), for $\hat{c} = 10$, the ratio of the critical stiffness to the critical stiffness for drained deformation (both based on the pore pressure p^0_∞) $K = 0.938$. Therefore, $\hat{c} = 10$ is close to drained conditions and there will be little difference in the response for larger values of $\hat{c}$. For $\hat{c} = 1$, $K = 0.51$, which is much closer to undrained response and, according to Figure 4 of Segall and Rice (1995), is in a range where $K(\hat{c})$ decreases rapidly with $\ln(\hat{c})$. For the parameters here undrained deformation is stable and the response is increasingly damped for smaller values of $\hat{c}$. Thus, the smaller peak velocities and stress drops in Figure 2, $\hat{c} = 1$, compared with Figure 3, $\hat{c} = 10$, reflect the stabilizing effects of dilatant hardening for conditions closer to undrained deformation.

For $\hat{c} = 0.1$, (see Supporting Information) $K = 0.09$, very close to undrained conditions. For $\dot{P}_\infty = 10^{-4}$, there are only a few small (maximum 1.3 v_0), slow (duration $\Delta T \approx 100$) slip events that decay quickly. For $\dot{P}_\infty = 10^{-3}$, there is one slow slip event with a peak velocity of about 3.7 v_0) which then decreases and levels off to a velocity of about 2.5 times the background rate. There are no discernible stress drops on the scale of the graph. For $\dot{P}_\infty = 10^{-3}$, there is still a significant downward trend to the stress that again reaches zero at $T = 800$. Responses for smaller values of $\hat{c}$ will be more strongly damped.

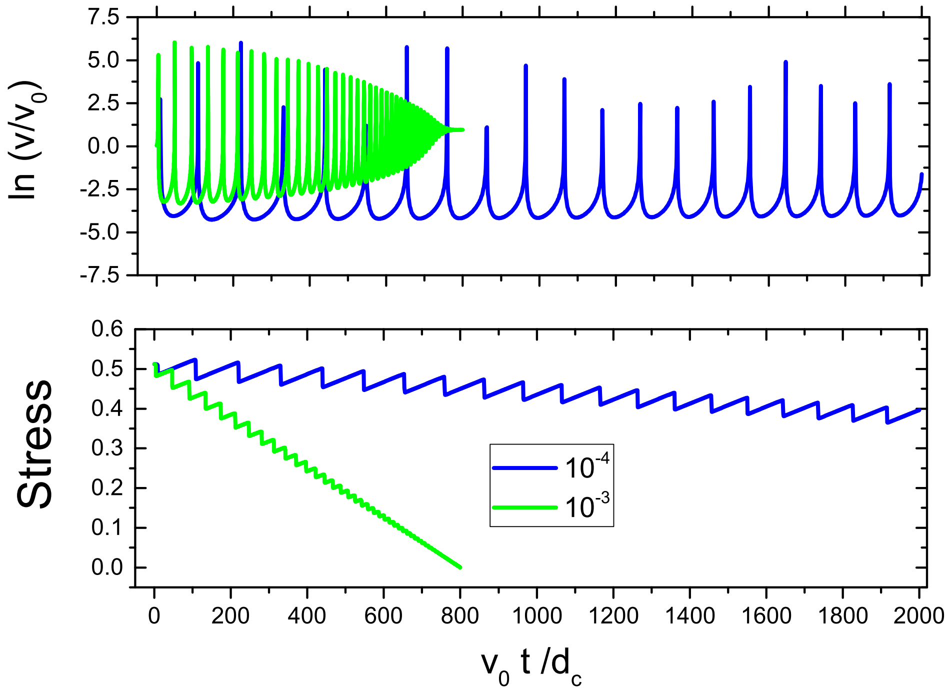

Figure 3. Same as Figure 2 for $\hat{c} = 10$.

Figure 4 shows the response for $\dot{P}_\infty = 10^{-2}$, representative of the laboratory value, for two values of $\hat{c}$: 1 and 10. The bottom panel shows that the frictional resistance decreases to zero at $T = 80$. For $\hat{c} = 10$, there are 12 slip events with slightly decreasing maximum slip rates before the end of the experiment ($T = 60$). The maximum slip rate is about 300 v_0, the maximum stress drop is about 3.1 MPa and the period is $\Delta T \approx 6$. For $\hat{c} = 1$, there is a single slow event followed by oscillations that are strongly damped because the response is closer to undrained deformation. For smaller diffusivities, the response is even more strongly damped.

5 Discussion

The simulations illustrate the effects of $\dot{P}_\infty$, the ratio of the characteristic time of the imposed rate of frictional slip to that of pressurization. For all the values of $\hat{c}$ and $\hat{k}$ considered, the frequency of events increases with $\dot{P}_\infty$. As the pore pressure in the reservoir increases, the effective stress decreases, reducing the value of k_{crit} (6) and stabilizing the response. Eventually, the effective stress goes to zero and the response is completely stabilized: the slip velocity returns to about the imposed rate. This limit is attained more quickly for larger $\dot{P}_\infty$. For $\dot{P}_\infty = 10^{-2}$, representative of the experiment of French et al. (2016) and similar to that of Wang et al. (2020) and the simulation of Almakari et al. (2019), it occurs about 30% beyond the end of the experiment. For $\dot{P}_\infty$ within the range of 10^{-4} to 10^{-3} the interaction of RS effects and the increase of pore pressure are most significant. For values smaller than this the pressure rate has little effect until very long times and the occurrence of slip events is dominated by RS effects.

The response also depends on $\hat{c}$, the ratio of the characteristic time of the imposed rate of frictional slip to that of fluid diffusion. The magnitude of the stress drop and peak velocities decrease with decreasing $\hat{c}$. The decrease is most dramatic for $\hat{c} = 0.1$, reflect-

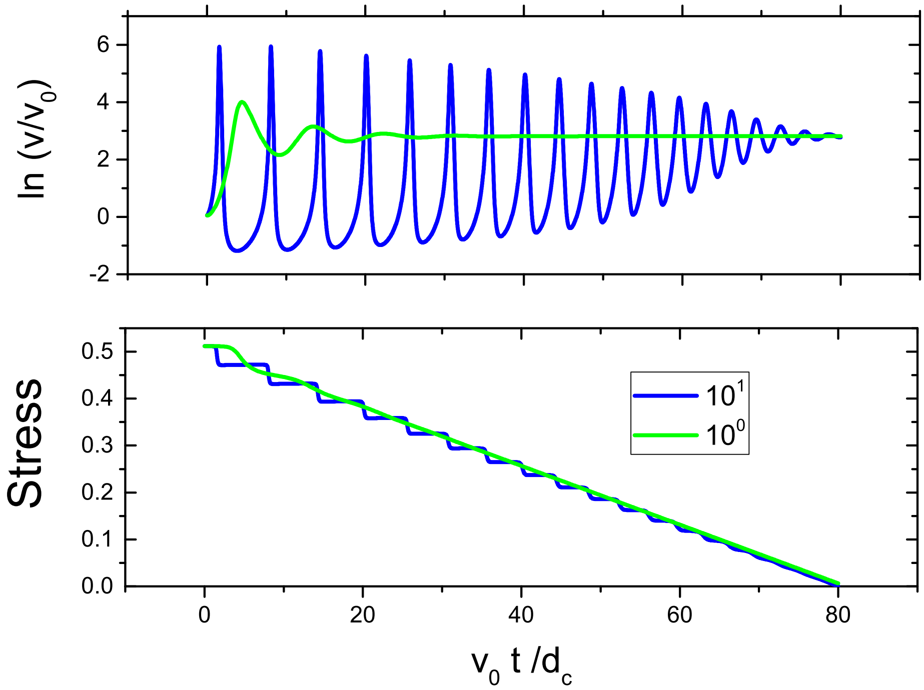

Figure 4. Same as Figure 2 for $\dot{P}_\infty = 10^{-2}$ and $\hat{c} = 1$ and 10.

ing the stabilizing effect of dilatant hardening as undrained conditions are approached. This stabilizing effect begins to dominate for $\hat{c}$ less than about 1. For $\hat{c}$ greater than about 10 conditions are effectively drained and largely independent of $\hat{c}$.

The analysis gives an indication of the possibility of slip instabilities in representative experiments. If we assume instabilities occur when the slip velocity is more than an order of magnitude greater than the background rate and must occur before the end of a representative experiment, $T = 60$, then they can occur only in a limited range of values of $\hat{k}$, $\hat{c}$ and $\dot{P}_\infty$. For $\hat{k} = 0.5$ (see Supporting Information) none occur because the peak slip velocities are too small. For $\hat{k} = 0.1$ none occur for $\hat{c} = 0.1$ because of the strong dilatant hardening when deformation is relatively undrained. For $\hat{c} = 10$ and $\hat{c} = 1$, instabilities occur only for $\dot{P}_\infty = 10^{-3}$ and 10^{-2}. These are in the range of the experiments of French et al. (2016), at least if the lower values of the permeability that they cite are appropriate.

Two other experiments that increase pressure in stepwise fashion at rates similar to those of French et al. (2016) are those of Wang et al. (2020) and Scuderi et al. (2017). The former use pressure rates of 2.0 MPa/min and 0.5 MPa/min. The latter use a smaller rate of 0.017 MPa/min. For $d_c = 0.02$ mm, $v_0 = 3.0 \times 10^{-7}$ m/s and $\sigma = 50$, the corresponding values of $\dot{P}_\infty$ are 0.044, 0.011 and 3.8×10^{-4}.

Another experiment imposing a pore pressure rate is that of Noël et al. (2019). They impose a sinusoidal pressure variation. Using the maximum pressure rate and other parameters from their experiment gives $\dot{P}_\infty$ in the range 0.015 to 0.120 for a displacement rate of 10^{-3} mm/s and an order of magnitude smaller for 10^{-4} mm/s. The range of $\dot{P}_\infty$ is where the rapid decrease of effective stress quickly stabilizes any instabilities due to RS effects. These estimates are consistent with their inference that the onset of slip corresponds to the reduction of the effective stress and that larger amplitudes induce the onset earlier.

The spring mass system is a primitive model of faulting. Nevertheless, we can make some connection with the study of Almakari et al. (2019). They simulate slip on a heterogeneous fault governed by RS friction and examine the seismicity rate increase due to a ramp increase in pore pressure at an injection site. The rates range from 0.01 to 10 MPa/day. $\sigma = 100$ MPa and $v_0 = 10^{-9}$ m/s. Their values of d_c vary along the fault and range from 0.01 to 0.37 mm. Using a value of $d_c = 0.1$ mm, in the middle of this range, a pressure rate 10 MPa/d and the values of σ and v_∞ yield $\dot{P}_\infty = 0.012$. This is about the same as for the French et al. (2016) experiment and at the upper range of where there is a competition between slip events due to RS friction and the rapid decrease of effective stress.

An important limitation of the simulations is that we have taken the normal stress as constant. In the standard axisymmetric compression tests changes of normal and shear stress are coupled by the geometry and in their experiments French et al. (2016) also alter the lateral stress which changes the normal stress on the slip surface. Rudnicki and Chen (1988) have used a slip-weakening model to examine the interaction of pore pressure effects with normal stress changes in experiments by Brace and Martin (1968) and Chambon and Rudnicki (2001) extended Segall and Rice (1995) to include normal stress changes. Neither of these studies included pore pressure rate changes. Another of changes in the normal stress neglected here is on state as identified by Linker and Dieterich (1992). This effect has been included in the simulations of Andrés et al. (2019) (although they did not look at the effect of pressure rate.

French et al. (2016) give some interpretation of their results in terms of RS effects but they do not measure values of the parameters a, b and d_c and the appropriate values are uncertain. Marone et al. (1990) found $d_c = 0.02$ mm from velocity stepping experiments on gouge layers of Ottawa sand and this value is probably reasonable for a sandstone. For a and b we have simply used representative magnitudes with $b > a$ in order to have velocity weakening and instability. Furthermore, there are indications that the values of a, b and d_c change with pore pressure and imposed slip rate (Scuderi & Collettini, 2016; Noël et al., 2019; Cappa et al., 2019).

In spite of the differences between the model and the experiment of French et al. (2016) the calculated stress drops and maximum slip rates are consistent with those observed in the experiments. For $\hat{c} = 10$ and $\dot{P}_\infty = 10^{-3}$ maximum slip rates are about two orders of magnitude greater than v_0, in rough agreement with the experiment (Figure 3d of French et al. (2016)). Similarly, stress drops from the calculations are similar to those in the experiments. Stress drops from Figure 4c of French et al. (2016) are 0.5 to 2.0 MPa. In the calculations they are slightly larger, about 3.0 to 4.0 MPa (0.04 to 0.05 $\times 50/\mu_0$ MPa). Admittedly, this agreement is based on the arbitrary choice of $\hat{k} = 0.1$. Maximum slip rates and stress drops for $\hat{k} = 0.5$ are much smaller. (See Supporting Information.)

There are, however, some clear discrepancies between the experiment and the simulations. French et al. (2016) observe a pore pressure increase, indicating compaction, accompanies slip instability. The magnitude of the increase is about 55 % of the shear stress drop and the increase is permanent. The simulations show a decrease of pressure with instability and then an increase with magnitude much smaller than observed in the experiment. One possible explanation is that the (nondimensional) pressure rate in the experiment is about 10^{-2} at which the rapid downward trend of the effective stress strongly stabilizes RS effects. Compaction and dilation in the formulation here, and in Segall and Rice (1995), are entirely associated with RS effects. (Segall and Rice (1995) remove a linear trend from the observations of Marone et al. (1990) to estimate RS parameters.)

The compaction observed by French et al. (2016) may be due to the neglect of normal stress changes in the simulations.

6 Conclusion

We have investigated the system of a spring and a mass sliding on a surface governed by RS friction. The pore pressure on the surface is coupled to the value in a remote reservoir. As Segall and Rice (1995) have shown, the model, although very simple, has a rich range of responses. The effects of increasing pore pressure in the reservoir further enrich this range. The analysis is motivated by observations that induced seismicity depends on injection rate and by experiments that examine the effect of pressure rate. The simulations illustrate the effects of pressure rate and diffusivity on the type, magnitude, frequency, and stress drop of slip events. Using parameters from the experiments of French et al. (2016) and Marone et al. (1990), we find that interaction of effects due to the pressure rate and RS friction are significant within a relatively narrow (a few orders of magnitude) range of pressure rates and diffusivity. Within this range, the frequency of slip events increases with increases in the pressure rate and maximum slip rates do not appear to be significantly affected by the pressure rate. More importantly, we find that RS instabilities are predicted to occur during the duration of an experiment only for a limited range of (non-dimensional) diffusivity and pressure rate. This range is similar to the pressure rates and diffusivities in the experiments of French et al. (2016), Noël et al. (2019), and Wang et al. (2020) and the field simulations of Almakari et al. (2019). Although the spring block configuration is simple, these simulations can aid in the interpretation of experiments and provide guidance for field studies.

Acknowledgments

No new data was used in this manuscript. Y.Z. thanks the University of Science and Technology Beijing for support and Northwestern University for hosting him during his visit from July 1, 2018 to January 1, 2019. JWR thanks Ghassan Shahin for assistance with the typesetting. We are grateful to reviewers Chris Marone and Paul Segall for their insightful comments that significantly improved the manuscript.

References

Almakari, M., Dublanchet, P., Hervé, C., & Frédéric, P. (2019). Effect of the injection scenario on the rate and magnitude content of injection-induced seismicity: Case of a heterogeneous fault. *Journal of Geophysical Research*, *124*, 8426-8448. doi: 10.1029/2019jb017898

Andrés, S., Santillán, D., Mosquera, J. C., & Cueto-Felgueroso, L. (2019). Delayed weakening and reactivation of rate-and-state faults driven by pressure changes due to fluid injection. *Journal of Geophysical Research*, *124*, 11,917-11,937. doi: 10.1029/2019.JB018109

Barbour, A. J., Norbeck, J. H., & Rubinstein, J. L. (2017). The effects of varying injection rates in Osage County, Oklahoma, on the 2016 Mw 5.8 Pawnee earthquake. *Seismological Research Letters*, *88*(4), 1040-1053.

Bhattacharya, P., Rubin, A. M., Bayart, E., Savage, H. M., & Marone, C. (2015). Critical evaluation of state evolution laws in rate and state friction: Fitting large velocity steps in simulated fault gouge with time-, slip-, and stress-dependent constitutive laws. *Journal of Geophysical Research*, *120*, 6365-6385. doi: 10.1002/2015JB012437

Brace, W. F., & Martin, R. J., III. (1968). A test of the law of effective stress for crystalline rocks of low porosity. *International Journal of Rock Mechanics and Mining Sciences*, *5*, 415-426.

Cappa, F., Scuderi, M. M., Collettini, C., Guglielmi, Y., & Avouac, J.-P. (2019).

Stabilization of fault slip by fluid injection in the laboratory and in situ. *Science Advances*, *5*(eaau4065). doi: 10.1126/sciadv.aau4065

Chambon, G., & Rudnicki, J. W. (2001). Effects of normal stress variations on frictional stability of a fluid-infiltrated fault. *Journal of Geophysical Research*, *106*(B6), 11,353-11,372.

Dieterich, J. H. (1979). Modeling of rock friction, 1, experimental results and constitutive equations. *Journal of Geophysical Research*, *84*, 2161-2168.

Ellsworth, W. L. (2013). Injection-induced earthquakes. *Science*, *341*. doi: 10.1126/science.1225942

French, M. E., Zhu, W., & Banker, J. (2016). Fault slip controlled by stress path and fluid pressurization rate. *Geophysical Research Letters*, *43*, 4330-4339. doi: 10.1002/2016GL068893

Goebel, T. H. W., Weingarten, M., X., C., Haffener, J., & Brodsky, E. E. (2017). The 2016 Mw 5.1 Fairview, Oklahoma earthquakes: Evidence for long-range poroelastic triggering at > 40 km from fluid disposal wells. *Earth and Planetary Science Letters*, *472*, 50-61. doi: 10.1016/j.epsl.2017.05.011

Green, D. H., & Wang, H. F. (1994). Shear wave velocity and attenuation from pulse-echo studies of Berea sandstone. *Journal of Geophysical Research*, *99*(B6), 11755 - 11763. doi: 10.10.1029/94JB00506

Horton, S. (2012). Disposal of hydrofracking waste fluid by injection into subsurface aquifers triggers earthquake swarm in central Arkansas with potential for damaging earthquake. *Seismological Research Letters*, *83*(2), 250-260. doi: 10.1785/gssrl.83.2.250

Keranen, K. M., Savage, H. M., Abers, G. A., & Cochran, E. S. (2013). Potentially induced earthquakes in Oklahoma, USA: Links between wastewater injection and the 2011 Mw 5.7 earthquake sequence. *Geology*, *41*(6), 699-702. doi: 10.1130G34045.1

Keranen, K. M., Weingarten, M., Abers, G. A., Bekins, B. A., & Ge, S. (2014). Sharp increase in central Oklahoma seismicity since 2008 induced by massive wastewater injection. *Science*, *345*(6195), 448-451. doi: 10.1126/science.1255802

Linker, M. F., & Dieterich, J. H. (1992). Effects of variable normal stress on rock friction: observations and constitutive equations. *Journal of Geophysical Research*, *97*, 4923-4940.

Marone, C. (1998). Laboratory - derived friction laws and their application to seismic faulting. *Annual Reviews of Earth and Planetary Science*, 643-696.

Marone, C., Raleigh, C. B., & Scholz, C. H. (1990). Frictional behavior and constitutive modeling modeling of simulated fault gouge. *Journal of Geophysical Research*, *95*, 7007 - 7025.

Noël, C., Passelégue, F. X., Giorgetti, C., & Violay, M. (2019). Fault reactivation during fluid pressure oscillations: Transition from stable to unstable slip. *Journal of Geophysical Research*, *124*, 10,940-10,953. doi: 10.1029/2019JB018517

Passelégue, F. X., Brantut, N., & Mitchell, T. M. (2018). Fault reactivation by fluid injection: controls from stress state and injection rate. *Geophysical Research Letters*, *45*, 12,837-12846. doi: 10.1029/2018GL080470

Rice, J. R. (1993). Spatio-temporal complexity of slip on a fault. *Journal of Geophysical Research*, *98*(B6), 9885-9907.

Rice, J. R., & Tse, S. T. (1986). Dynamic motion of a single degree of freedom system following a rate and state dependent friction law. *Journal of Geophysical Research*, *91*(B1), 521-530.

Rudnicki, J. W., & Chen, C.-H. (1988). Stabilization of rapid frictional slip on a weakening fault by dilatant hardening. *Journal of Geophysical Research*, *93*, 4745-4757.

Ruina, A. (1983). Slip instability and state variable friction laws. *Journal of Geophysical Research*, *88*, 10,359-10,370.

Scuderi, M. M., & Collettini, C. (2016). The role of fluid pressure in induced vs. triggered seismicity: insights from rock deformation experiments on carbonates. *Nature Scientific Reports*. doi: 10.1038/srep24852

Scuderi, M. M., Collettini, C., & Marone, C. (2017). Frictional stability and earthquake triggering during fluid pressure stimulation of an experimental fault. *Earth and Planetary Science Letters*, *477*, 84-96.

Segall, P., & Rice, J. R. (1995). Dilatancy, compaction, and slip instability of a fluid-infiltrated fault. *Journal of Geophysical Research*, *100*(B11), 22155-22171.

Wang, L., Kwiatek, G., Rybacki, E., Bonnelye, A., Bohnhoff, M., & Dresen, G. (2020). Laboratory study on fluid-induced fault slip behavior: The role of fluid pressurization rate. *Geophysical Research Letters*, *47*(e2019GL086627). doi: 10.1029/2019GL086627

Weingarten, M., Ge, S., Godt, J. W., Bekins, B. A., & Rubinstein, J. L. (2015). High-rate injection is associated with the increase in U.S. mid-continent seismicity. *Science*, *348*(6241), 1336-1340.

Wibberley, C. A. J., & Shimamoto, T. (2003). Internal structure and permeability of major fault zones: The Median Tectonic Line in Mie Prefecture, Southwest Japan. *Journal of Structural Geology*, *25*, 49-78.

Zhang, S., & Tullis, T. (1998). The effect of fault slip on permeability and permeability anisotropy in quartz gouge. *Tectonophysics*, *298*(1-2), 41-52.

Zoback, M. D., & Byerlee, J. D. (1976). Effect of high-pressure on permeability of Ottawa sand. *American Association of Petroleum Geologists Bulletin*, *60*, 1531-1542.

Supporting Information for "Effect of Pressure Rate on Rate and State Frictional Slip"

J. W. Rudnicki[1]and Y. Zhan[2]

[1]Department of Civil and Environmental Engineering and Department of Mechanical Engineering, Northwestern University, Evanston, IL 60208-3109

[2]School of Civil and Resource Engineering, University of Science and Technology Beijing, No.30, Xueyuan Road, Haidian District, Beijing, 100083, P. R. China

This supporting information presents additional simulations not included in the text. The first is the same as Figure 2 of the text, but for a smaller value of the diffusivity $\hat{c} = 0.1$. The three others are the same simulations as in Figures 2, 3, and 4 of the text for a larger value of the ratio of the spring stiffness to the critical value for drained deformation (eqn. (6) of the text), in particular, $\hat{k} = 0.5$.

The results for $\hat{c} = 0.1$ and $\hat{k} = 0.1$ are shown in Figure S1. The value of $K = 0.09$, eqn. (9) of text, is close to undrained conditions, and as a result, the response is strongly stabilized. For $\dot{P}_\infty = 10^{-3}$, there is one slow slip event with a peak velocity of about $3.7v_0$

Corresponding author: J. W. Rudnicki, Department of Civil and Environmental Engineering, Northwestern University, Evanston, IL 60208-3109, USA jwrudn@northwestern.edu

(which may be affected by the initial condition). The velocity quickly decays and levels off at about $2.6v_0$. (The velocity does not decay completely back to v_0 because the pressure rate is non-zero.) For $\dot{P}_\infty = 10^{-4}$, the maximum slip velocity is only $1.15v_0$. After a few small, slow events the velocity levels off at $1.15v_0$. Stress drops are not discernible on the scale of the graph. Responses for smaller values of $\hat{c}$ will be even more strongly damped.

The results for $\hat{k} = 0.5$ are shown in Figure S2 for $\hat{c} = 1$ and in Figure S3 for $\hat{c} = 10$. Figure S4 shows results for $\dot{P}_\infty = 10^{-2}$ and two values of $\hat{c}$: 1.0 and 10.0. Because the effective stress goes to zero at $T = 80$ the simulation is stopped there. Compared with $k = 0.1$, the results for $k = 0.5$ have lower maximum velocities and stress drops and higher frequencies. As for $k = 0.1$, maximum velocities increase and frequencies decrease with decreasing $\dot{P}_\infty$

The upper panel of Figure S2 shows that the slip events are frequent but the maximum velocities are small, no greater than about 2.7 v_0. For $\dot{P}_\infty = 10^{-3}$ the velocity is strongly damped because of the rapid decrease of the effective stress. For $\dot{P}_\infty = 10^{-4}$ and 10^{-5}, the velocities initially increase. They appear to reach a steady oscillation but they will eventually decline because of the increasing pore pressure. The amplitudes slowly increase and decrease. The lower panel shows the stress. The stress drops for $\dot{P}_\infty = 10^{-3}$ are indiscernible on the scale of the graph. For $\dot{P}_\infty = 10^{-4}$ and 10^{-5}, the pore pressure increases so slowly that the stress appears to be nearly constant and the drops in stress appear as small ripples.

For Figure S3 $\hat{c} = 10$. Conditions are nearly drained and there is little stabilization due to dilatant hardening. Maximum slip velocities are about 30 v_0. As in Figure S2, the more rapid decrease of the effective stress for $\dot{P}_\infty = 10^{-3}$ damps the response. For $\dot{P}_\infty = 10^{-4}$ and 10^{-5} the velocity appears to become periodic and the stress appears nearly constant but both will eventually decline. Stress drops are very small.

For $\dot{P}_\infty = 10^{-2}$ in Figure S4 the response is strongly damped. For $\hat{c} = 10$, there is a series of events with the peak velocities decaying from a maximum of 30 v_0 to 4.3 v_0 at $T \approx$. For $\hat{c} = 1$ there are only one or two small, slow events. Stress drops are not discernible for $\hat{c} = 1$ and only small ripples for $\hat{c} = 10$.

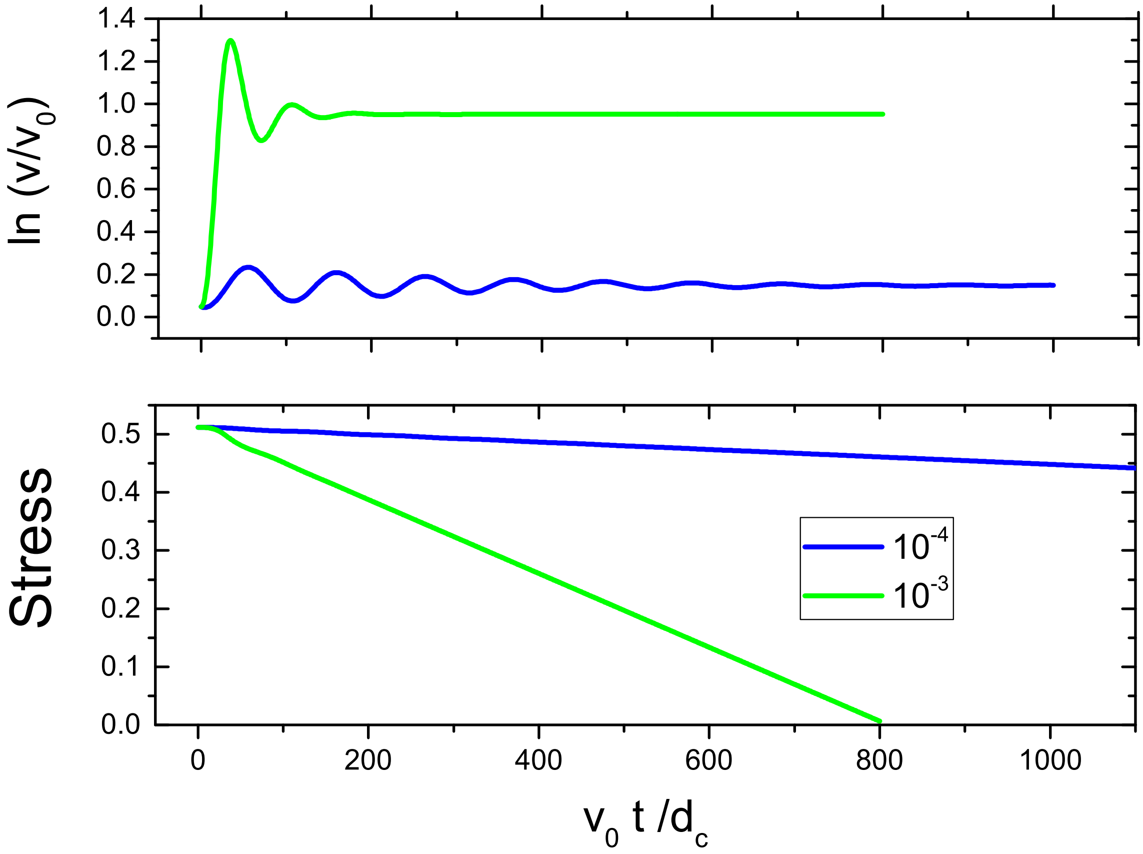

Figure S1. Upper panel shows logarithm of velocity (divided by v_0) and lower panel shows stress (divided by σ), $\Sigma = \mu_0 (1 - p/\sigma)$, for two values of $\hat{P}_\infty$: 10^{-4} and 10^{-3} The abscissa is $T = v_0 t/d_c$ and $\hat{c} = 0.1$ and $\hat{k} = 0.1$.

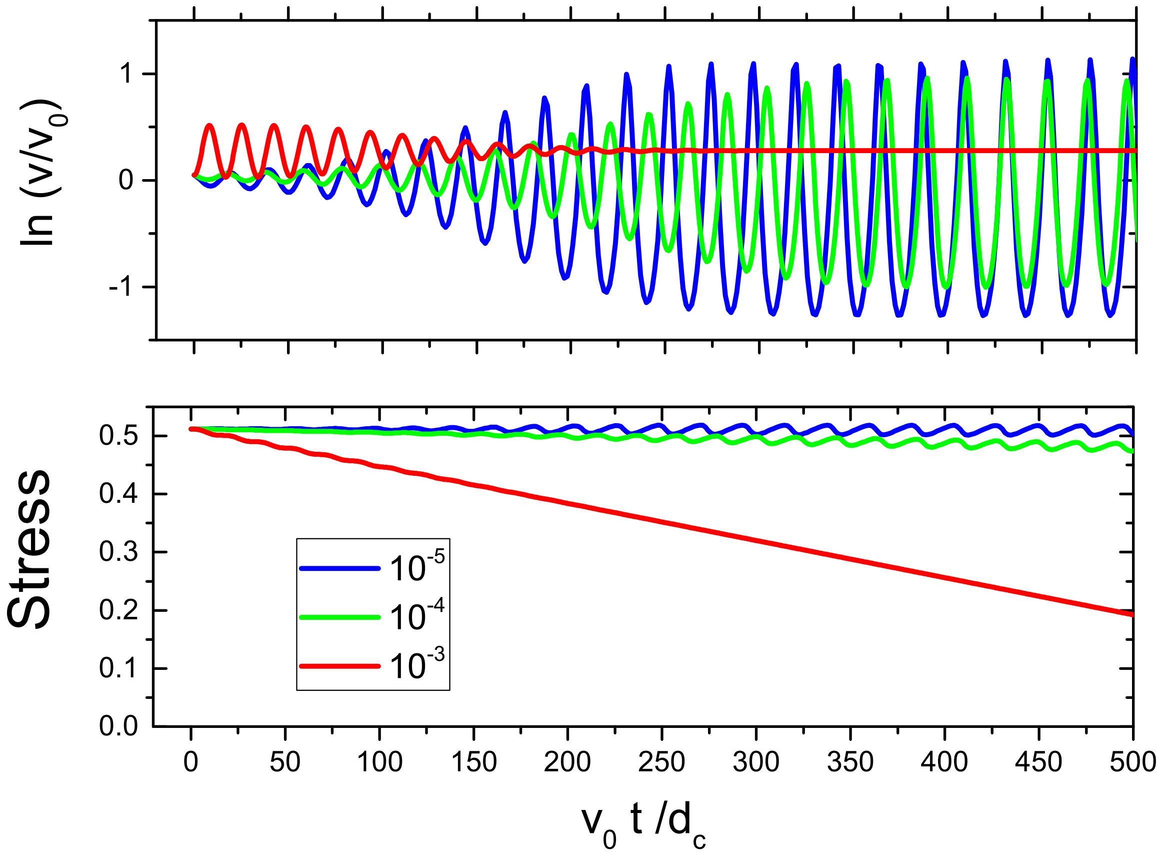

Figure S2. Same as Figure 2 of text except $\hat{k} = 0.5$. Upper panel shows logarithm of velocity (divided by v_0) and lower panel shows stress (divided by σ), $\Sigma = \mu_0\,(1 - p/\sigma)$, for three values of $\hat{P}_\infty$: 10^{-5}, 10^{-4} and 10^{-3} The abscissa is $T = v_0 t/d_c$ and $\hat{c} = 1$.

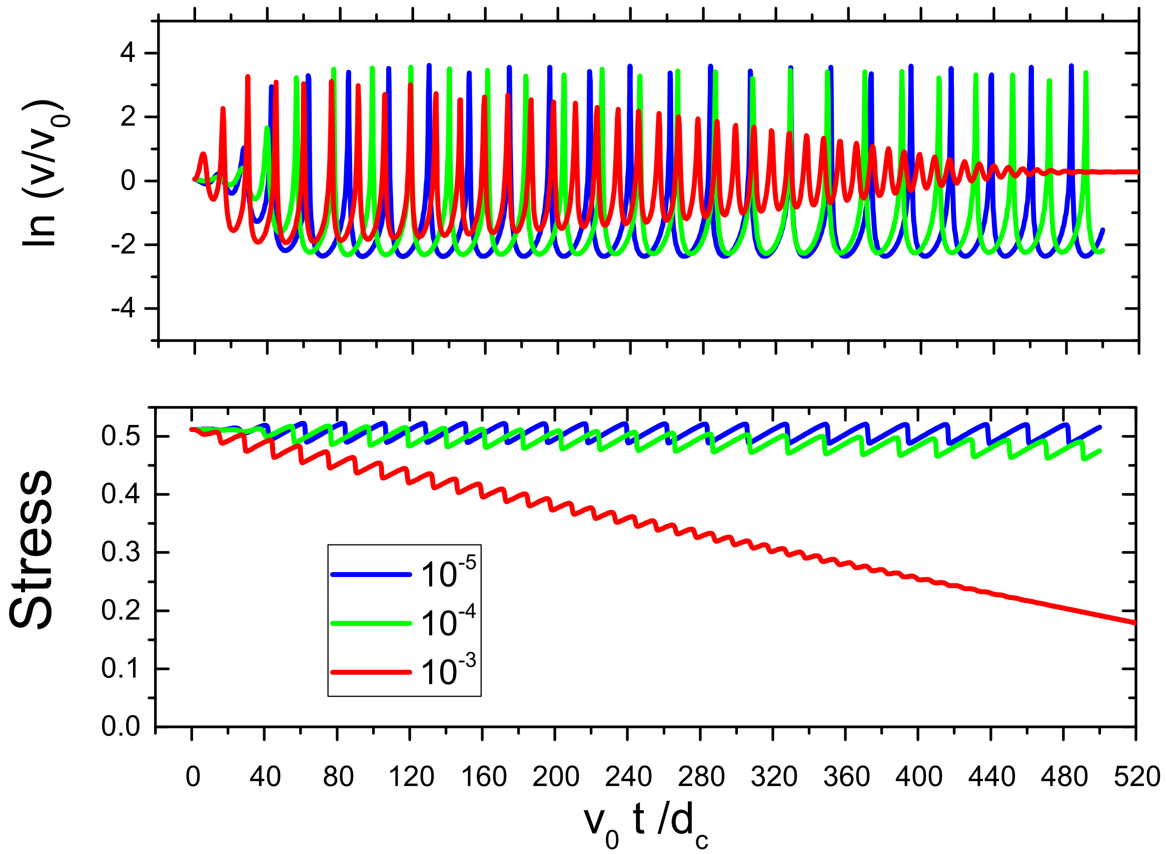

Figure S3. Same as Figure S2 for $\hat{c} = 10$.

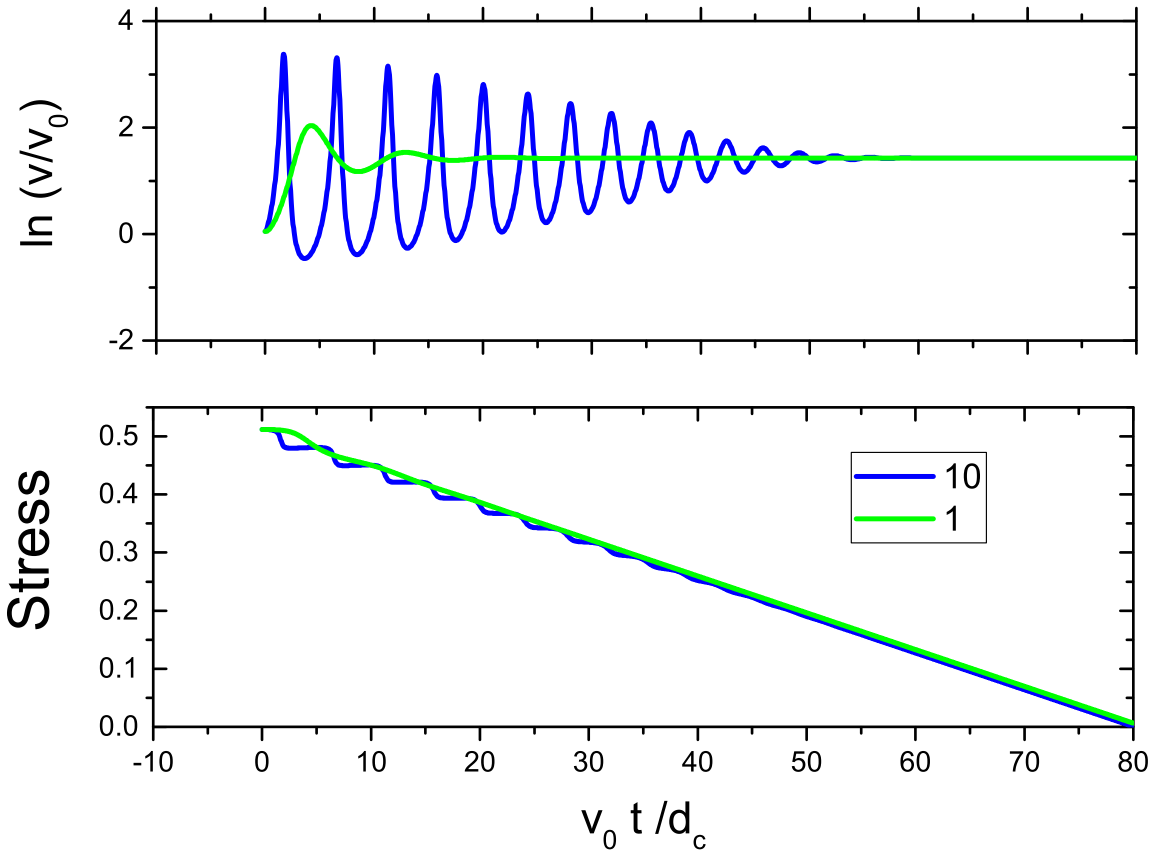

Figure S4. Same as Figure S2 for $\dot{P}_\infty = 10^{-2}$ and $\hat{c} = 1$ and 10.